Eur. Phys. J. C (2025) 85:966
https://doi.org/10.1140/epjc/s10052-025-14698-6

THE EUROPEAN PHYSICAL JOURNAL C

Regular Article - Theoretical Physics

Stable anisotropic solutions for compact stars in matter-geometry coupled theory under some specific spacetimes

Tayyab Naseer[1,2,a], **M. Sharif**[1,b], **M. Waqas**[1,c], **Nazek Alessa**[3,d], **Mohamed R. Eid**[4,e]

[1] Department of Mathematics and Statistics, The University of Lahore, 1-KM Defence Road, Lahore 54000, Pakistan
[2] Research Center of Astrophysics and Cosmology, Khazar University, 41 Mehseti Street, AZ1096 Baku, Azerbaijan
[3] Department of Mathematical Sciences, College of Science, Princess Nourah bint Abdulrahman University, P.O. Box 84428, Riyadh 11671, Saudi Arabia
[4] Center for Scientific Research and Entrepreneurship, Northern Border University, Arar 73213, Saudi Arabia

Received: 23 May 2025 / Accepted: 29 August 2025

Abstract This article examines how compact astronomical objects behave under the theoretical framework of $f(R, L_m, T)$ theory of gravity. We develop modified field equations by taking into consideration the static internal spacetime which is filled with the anisotropic fluid content. Applying two particular constraints related to the anisotropic pressure and radial metric function allows us to identify two new solutions to these gravitational equations. We obtain differential equations for both models, the integration of which yields constants that are established using matching criteria. The necessity for radial pressure to vanish at the hypersurface is also used to find these constants. Afterwards, for various values of the parameters involved in the considered modified model, we visually assess certain requirements whose fulfillment guarantees the viability of the model. For this purpose, we consider the observational data of a compact star 4U 1820-30. We deduce that both of our models meet the necessary stability and viability requirements. Notably, our study advances the understanding of compact stellar models by demonstrating how the considered theory of gravity modifies their evolutionary pattern compared to general relativity, and provides a robust framework for exploring matter-geometry coupling in future astrophysical research.

1 Introduction

General relativity (GR) gives us a mathematical foundation to study the universe, particularly regions with extremely dense and massive objects. This theory explains the connection between the matter dispersion that creates the curvature and the gravitational field it produces. The interior of a self-gravitating body is represented by non-linear Einstein field equations, which explain this behavior. Understanding the behavior of compact astrophysical phenomena requires scientists to solve Einstein's field equations, either through numerical or exact methods. In 1916, Karl Schwarzschild made a ground-breaking contribution to astrophysics by deriving the first exact solution to Einstein's field equations describing a non-rotating, spherically symmetric massive object. Schwarzschild derived distinct metric solutions for both the vacuum region outside and the interior of a static, perfect fluid sphere with uniform energy density, as documented in his seminal works [1,2]. Subsequent analysis revealed that Schwarzschild's solution exhibited a mathematical singularity at $r = 0$, indicating a breakdown of the coordinate system at the central point of the gravitational source. Later research has shown that our universe includes a significant quantity of dark energy, an enigmatic force that causes the rapid cosmic expansion. Although GR sheds light on this phenomenon, it fails to fully explain the cosmological constant. Researchers have thus focused to find a theoretical framework to define gravity in a better way and to solve the inconsistencies linked with Einstein's theory.

Several modified theories, in this context, have been proposed in the literature which produced promising results in cosmological scenarios. By substituting a generalized function of the Ricci scalar R in place of the geometric component

[a] e-mails: tayyab.naseer@math.uol.edu.pk; tayyab.naseer@khazar.org; tayyabnaseer48@yahoo.com (corresponding author)
[b] e-mail: msharif.math@pu.edu.pk
[c] e-mail: mw973021@gmail.com
[d] e-mail: naalessa@pnu.edu.sa
[e] e-mail: mohamed.eid@nbu.edu.sa

Published online: 10 September 2025

of the conventional Einstein–Hilbert action, the first simple modification of GR, known as $f(R)$ theory, was developed. To explain the universe's present fast expansion and inflationary epoch, many scholars have investigated this theory and found it favorable [3,4]. Several $f(R)$ models' stable behavior has been examined using a variety of mathematical approaches [5–7]. The idea of matter-geometry interaction was later developed mainly by Bertolami et al. [8] inside the action of $f(R)$ theory. They introduced the $f(R, L_m)$ theory by combining the Lagrangian density and the geometrical quantity R into a single function. The changes in the physical characteristics of celestial bodies have been noticed due to this alteration, see for instance the works done in [9–12]. Building on these developments, Harko et al. [13] introduced $f(R, T)$ gravity – a modified theory of gravitation where the action is generalized to an arbitrary function of R and the trace T of the energy-momentum tensor (EMT). The existence of an exotic fluid has been blamed for the functional-dependence on T.

Notably, when the fluid term T is added in the action function, the non-conservation phenomenon occurs, which results in the presence of additional force. The particles' non-geodesic motion is thus caused by this force, which stops test particles from following a geodesic path. This theory has been shown to produce many significant cosmological and astrophysical ramifications [14–21]. Despite offering a potential solution to cosmic riddles, $f(R, T)$ gravity faces many substantial barriers. For instance, this theory makes it difficult to construct viable models that simultaneously satisfy both cosmological constraints and local-scale gravitational tests. This enabled Harko and Haghani [22] to integrate the $f(R, T)$ and $f(R, L_m)$ gravity models in a single function, and named this theory as $f(R, L_m, T)$ gravity. In this framework, two distinct models – minimal and non-minimal – have been examined, and the resulting findings are found to be in agreement with the data. The minimal model of this theory yields superior findings in comparison with the other, according to study done by Naseer and Said [23], who investigated the inner structure of charged isotropic stars. Some significant studies showing this theory's theoretical and observational efficacy are [24–32].

It is important to note that the $f(R, L_m, T)$ gravitational framework can be evaluated within the post-Newtonian regime to verify its alignment with empirical checks in the solar system, including phenomena like Mercury's orbital advance or the delay in light propagation known as the Shapiro effect. Under the low-gravity assumption, the governing equations for this theory may be developed as expansions from flat Minkowski geometry, where deviations are described through gravitational potentials and the framework's interaction coefficients. When the coefficients in various forms of this theory – responsible for regulating the linkage between matter and spacetime – are kept minimal, the extra contributions to the equations fade into the background, causing the theory to align with GR at the primary level of the post-Newtonian series. This alignment guarantees compliance with the parameterized post-Newtonian (PPN) limits, which are rigorously restricted by data from solar system studies. As an example, the PPN factor γ, quantifying the spatial bending caused by a given mass, must lie within 10^{-5} of 1 according to signal propagation timing data. Through precise tuning of the framework's coefficients to remain modest in solar system scenarios, the $f(R, L_m, T)$ model produces γ values close to 1, matching these empirical findings. Regarding dense stellar objects, the coefficients can avoid being extremely tiny while still yielding meaningful physical insights. Within regions of elevated density, the interaction elements in modified gravitational equations gain prominence, resulting in departures from GR that account for features like uneven matter arrangements and equilibrium traits in such stars. The chosen magnitudes avoid being excessive enough to undermine agreement with GR in low-gravity settings, yet they are substantial enough to prevent the alterations from becoming negligible. Consequently, the framework achieves an equilibrium by incorporating fresh gravitational influences in intense-field areas while preserving observational reliability in milder gravitational conditions.

In any theory of gravity, the equilibrium configuration of a self-gravitating system is completely determined by solving the corresponding field equations, which govern both the spacetime geometry and matter distribution. The complexity of solving the field equations increases substantially with the incorporation of higher-order geometric derivatives. Based on the scenario, the solution could be numerical or analytical, and initial/boundary conditions are needed in the former case. To get a complete solution, however, further data on local physics is required. Several newly identified elements impact the structural characteristics of these large bodies in the study of stellar implosion [33–35]. The system of three independent gravitational field equations for a static anisotropic sphere contains five unknown quantities (two metric coefficients and three matter terms). Without specifying additional conditions like a particular metric ansatz, obtaining exact solutions to this under-determined system remains theoretically challenging. A well-behaved solution may be obtained by reducing the number of unknowns or by restricting the metric coefficients. Several studies have employed the Karmarkar requirement, a geometric constraint that establishes a differential relationship between the two metric potentials, enabling the derivation of one gravitational potential from the other [36]. The solution has also been explored in the context of stellar systems under the vanishing Weyl tensor [37].

Earlier theoretical models assumed that spherically symmetric celestial fluid systems exhibited perfectly isotropic matter distributions, implying identical pressure magnitudes

regardless of directional orientation. Based on Jeans' fundamental study [38], the fluid must exhibit directional dependence in its properties which is because the interior geometry is influenced by a number of elements. Ruderman [39] demonstrated that stellar objects exceeding densities of $10^{15}\ g/cm^3$ exhibit unequal pressure components. Canuto [40] pointed out that the anisotropy might result from differences in radial and transverse pressures caused by the exceptionally high density of compact stars. Strong magnetic fields [41], pion condensation [42], nuclear interaction [43], superfluid core [44], and other factors may all result in anisotropy inside these structures. Bowers and Liang [45] investigated how anisotropy affected the equilibrium of celestial formations and came to the conclusion that anisotropy should vanish at the star's core. Three key concepts form the basis of the Bowers–Liang model are that the anisotropy must (i) disappear at the center, (ii) be induced by the gravitational impact, and *(iii)* not be linearly connected to the radial pressure [46]. Using a particular anisotropic factor, Sharif and Naseer [47] obtained anisotropic solutions, and their findings were in good agreement with the physical criteria. Some interesting studies on different compact stars under multiple approaches can be found in [48–58].

The existing solutions are extended in this study within the context of $f(R, L_m, T)$ theory under the approach used in [59,60]. The structure of the paper is arranged as follows. The next section presents the fundamentals of the considered modified gravity and formulates the field equations for a static sphere permeated by the anisotropic fluid. Two innovative stellar models are formulated by taking into account a couple of radial potentials and certain types of anisotropy in Sect. 3. The matching requirements between the Schwarzschild external and the internal spherical metrics are also applied which aids in the computation of constants involved in the resulting solutions. Afterwards, through graphical analysis, we confirm the fulfillment of many physical requirements that must be met for a solution to be acceptable in Sects. 4 and 5. Section 6 then comprises a brief discussion of the developed results for different parametric values. Finally, Sect. 7 provides a thorough review of our findings and highlights key achievements.

2 Modified gravity theory

The $f(R, L_m, T)$ gravitational framework introduces modifications to the conventional Einstein-Hilbert action as follows

$$S_{f(R,L_m,T)} = \int \sqrt{-g}\left\{\frac{f(R, L_m, T)}{16\pi} + L_m\right\} d^4x, \tag{1}$$

where the Lagrangian density for the matter distribution is denoted by L_m. The field equations may be obtained using the least-action approach on the action (1) as

$$G_{\alpha\beta} = 8\pi T^{(eff)}_{\alpha\beta}, \tag{2}$$

where $T^{(eff)}_{\alpha\beta}$ is an effective EMT and $G_{\alpha\beta} = R_{\alpha\beta} - \frac{1}{2}Rg_{\alpha\beta}$ represents the Einstein tensor. The former term is given by

$$T^{(eff)}_{\alpha\beta} = \frac{1}{f_R}T_{\alpha\beta} + T^{(D)}_{\alpha\beta}. \tag{3}$$

Here, the normal matter EMT is shown by the term $T_{\alpha\beta}$, and the involvement of modified corrections as a result of altering the action function is presented by $T^{(D)}_{\alpha\beta}$ which is expressed below

$$\begin{aligned} T^{(D)}_{\alpha\beta} = \frac{1}{8\pi f_R}\Bigg[&\frac{1}{2}(2f_T + f_{L_m})T_{\alpha\beta} + \frac{1}{2}(f - Rf_R)g_{\alpha\beta} \\ &- (g_{\alpha\beta}\Box - \nabla_\alpha\nabla_\beta)f_R - \frac{1}{2}(2f_T + f_{L_m})L_m g_{\alpha\beta} \\ &+ 2f_T g^{\xi\mu}\frac{\partial^2 L_m}{\partial g^{\alpha\beta}\partial g^{\xi\mu}}\Bigg]. \end{aligned} \tag{4}$$

A fundamental mathematical construct for describing the intrinsic spacetime geometry of astrophysical bodies is the metric. To properly analyze the dynamics of matter and energy distributions in gravitationally bound systems, one must first establish this fundamental geometric description. The static spherical metric offers significant advantages for solving gravitational field equations, primarily through mathematical simplification. The assumption of spherically symmetric geometry significantly reduce the complexity of the governing equations, enabling more compliant study and solution of physical problems. In our ongoing analysis, we consider the internal spacetime described by

$$ds^2 = -B_1^2(r)dt^2 + B_2^2(r)dr^2 + r^2(d\theta^2 + \sin^2\theta d\phi^2), \tag{5}$$

where the aforementioned metric's static character is shown by only the r-dependence of its components.

Researchers studying a variety of physical processes have paid a close attention to the anisotropic fluid interiors. This recognizes the directional dependencies present in energy and momentum distributions, in contrast to their isotropy equivalents, which suppose uniform qualities in every direction. This difference is crucial for modeling systems with orientation-dependent properties, including spinning bodies or surroundings with strong gravitational fields. We investigate the anisotropic matter dispersion represented by EMT given below

$$T_{\alpha\beta} = (\rho + p_t)v_\alpha v_\beta + p_t g_{\alpha\beta} - \big(p_r - p_t\big)u_\alpha u_\beta. \tag{6}$$

Here, the energy density, radial, and transverse/tangential pressure are denoted by ρ, p_r, and p_t, respectively. Additionally, u_α denotes the 4-vector along the radial direction,

and v_β is the 4-velocity. They have the following form in regard to the line element (5) in a co-moving frame of reference

$$v_\alpha = \big(-B_1(r), 0, 0, 0\big), \quad u_\alpha = \big(0, B_2(r), 0, 0\big), \tag{7}$$

fulfilling certain relationships provided by

$$v^\alpha u_\alpha = 0, \quad v^\alpha v_\alpha = -1, \quad u^\alpha u_\alpha = 1.$$

Choosing a particular modified gravity model allows researchers to address GR's limitations in explaining cosmic events, which is crucial for generating significant breakthroughs in cosmological and astrophysical studies. Furthermore, the selection of a modified gravity model influences future experiment design as well as the interpretation of current data, making it a crucial issue in contemporary astrophysics. Among the several $f(R, L_m, T)$ models documented in the literature, we choose the linear one defined by

$$\begin{aligned} f(R, L_m, T) &= R + \alpha f_1(R) + 2\gamma f_2(L_m) + \lambda f_3(T) \\ &= R + 2\gamma L_m + \lambda T, \end{aligned} \tag{8}$$

under dimensionless constants γ and λ which shall be chosen as specific values in subsequent analysis. The $f(R, L_m, T)$ gravitational framework provides a more comprehensive approach for modeling dark energy phenomena compared to traditional paradigms such as quintessence fields. Cosmic acceleration is simply described by traditional dark energy models, which usually require a certain kind of dynamic energy density or a constant energy density. However, by including not just the Ricci scalar but also the matter Lagrangian and the trace of the EMT, the functional $f(R, L_m, T)$ enables a more comprehensive interaction between geometry and matter. To accurately model the interior dynamics of dense stellar objects such as compact stars, researchers must employ nonlinear gravitational field equations. These equations account for anisotropic pressure distributions and variations in energy density, which are critical for understanding the structural evolution of these astrophysical bodies.

The adoption of a linear model (8) offers several distinct advantages when modeling the complex internal structures of anisotropic compact stars. Unlike non-linear $f(R)$ models, which introduce higher-order curvature terms that significantly increase the complexity of the field equations, the linear model simplifies the mathematical framework while still capturing essential interactions between geometry, matter, and the trace of EMT. This simplicity is particularly beneficial in the context of anisotropic stars, where the interplay between radial and tangential pressures adds additional degrees of freedom to the system. Non-linear $f(R)$ models, such as $f(R) = R + \alpha R^2$, often lead to highly non-linear differential equations that are challenging to solve analytically, especially when coupled with anisotropic fluid distributions. These complexities can obscure physical insights and require numerical methods, which may introduce uncertainties in interpreting the results. In contrast, the considered model in this case allows for analytical solutions, enabling precise control over the metric potentials and fluid parameters. This facilitates a clearer understanding of how the modified gravity terms influence the stellar structure, making it easier to derive physically meaningful constraints and test the model against observational data, such as that of the compact star 4U 1820-30.

Another key benefit of the linear model (8) is its ability to incorporate both the matter Lagrangian and the trace of EMT in a straightforward manner, providing a more comprehensive description of matter-geometry coupling compared to $f(R)$ or $f(R, T)$ theories. The $f(R)$ theory focuses solely on curvature modifications, neglecting direct interactions with the matter sector, which can limit its ability to model complex anisotropic effects in compact stars. The $f(R, T)$ theory includes the trace T, introducing non-conservation effects that lead to non-geodesic motion, but it does not account for the matter Lagrangian's contribution, which is critical for describing the internal dynamics of dense objects with anisotropic pressures. The $f(R, L_m, T)$ model, by contrast, allows for a richer description of the interplay between geometry and matter. This is particularly relevant for anisotropic stars, where directional pressure differences arise from physical processes like strong magnetic fields, pion condensation, or nuclear interactions. The linear form ensures that these additional terms introduce manageable corrections to the Einstein field equations, preserving the physical interpretability of the solutions while accounting for deviations from GR.

In addition, classical models often depend on certain assumptions on the dark energy equation of state, whereas $f(R, L_m, T)$ theory allows for adjustments that may rely on the local matter dispersion and shape, giving greater leeway in describing dark energy dynamics. This leads to solutions that better match the observed data from compact astronomical objects. Incorporating anisotropic stress tensors and gravitational potential terms into the modified Einstein field equations allows for a more robust analysis of compact stars' stability and viability across varying astrophysical regimes. This framework demonstrates that $f(R, L_m, T)$ gravity theories can yield deeper theoretical insights compared to standard dark energy models.

When we combine Eqs. (2), (6), and (8), the spherically symmetry metric (5) yields the following field equations, which govern the system's evolution as

$$(8\pi+\gamma+\lambda)\rho-\lambda\left(\frac{p_r}{6}+\frac{p_t}{3}-\frac{\rho}{2}\right)=\frac{2B_2'(r)}{rB_2(r)^3}-\frac{1}{r^2B_2(r)^2}+\frac{1}{r^2}, \tag{9}$$

Anisotropy is the result of pressure's changes in different directions within a fluid dispersion. We look at two distinct orientations in this analysis, namely tangential and radial. Consequently, the definition of the anisotropic factor becomes

$$\Pi(r)=p_t-p_r=\frac{B_1(r)\left\{B_2(r)^3-B_2(r)-rB_2'(r)\right\}-r\left\{rB_1'(r)B_2'(r)+B_2(r)\left(B_1'(r)-rB_1''(r)\right)\right\}}{r^2(\gamma+\lambda+8\pi)B_1(r)B_2(r)^3}. \tag{15}$$

$$(8\pi+\gamma+\lambda)p_r+\lambda\left(\frac{p_r}{6}+\frac{p_t}{3}-\frac{\rho}{2}\right)=\frac{2B_1'(r)}{rB_1(r)B_2(r)^2}+\frac{1}{r^2B_2(r)^2}-\frac{1}{r^2}, \tag{10}$$

$$(8\pi+\gamma+\lambda)p_t+\lambda\left(\frac{p_r}{6}+\frac{p_t}{3}-\frac{\rho}{2}\right)=-\frac{B_2'(r)}{rB_2(r)^3}+\frac{1}{B_1(r)B_2(r)^2}\times\left(B_1''(r)-\frac{B_1'(r)B_2'(r)}{B_2(r)}+\frac{B_1'(r)}{r}\right). \tag{11}$$

The fluid parameters may be obtained in their explicit form from the aforementioned equations as

$$\begin{aligned}\rho=&\frac{1}{3r^2(\gamma+\lambda+8\pi)(\gamma+2\lambda+8\pi)B_1(r)B_2(r)^3}\\&\times\left[\lambda r^2B_1'(r)B_2'(r)-\lambda r^2B_2(r)B_1''(r)-2\lambda rB_2(r)B_1'(r)\right.\\&-6\gamma rB_1(r)B_2'(r)-8\lambda rB_1(r)B_2'(r)-48\pi rB_1(r)B_2'(r)\\&-3\gamma B_1(r)B_2(r)^3+3\gamma B_1(r)B_2(r)-4\lambda B_1(r)\\&\times B_2(r)^3+4\lambda B_1(r)B_2(r)\\&\left.-24\pi B_1(r)B_2(r)^3+24\pi B_1(r)B_2(r)\right],\end{aligned} \tag{12}$$

$$\begin{aligned}p_r=&\frac{1}{3r^2(\gamma+\lambda+8\pi)(\gamma+2\lambda+8\pi)B_1(r)B_2(r)^3}\\&\times\left[\lambda r^2B_1'(r)B_2'(r)-\lambda r^2B_2(r)B_1''(r)+6\gamma rB_2(r)B_1'(r)\right.\\&+10\lambda rB_2(r)B_1'(r)+48\pi rB_2(r)B_1'(r)+4\lambda rB_1(r)B_2'(r)\\&-3\gamma B_1(r)B_2(r)^3+3\gamma B_1(r)B_2(r)-4\lambda B_1(r)\\&\times B_2(r)^3+4\lambda B_1(r)B_2(r)\\&\left.-24\pi B_1(r)B_2(r)^3+24\pi B_1(r)B_2(r)\right],\end{aligned} \tag{13}$$

$$\begin{aligned}p_t=&\frac{1}{3r^2(\gamma+\lambda+8\pi)(\gamma+2\lambda+8\pi)B_1(r)B_2(r)^3}\\&\times\left[3\gamma r^2B_2(r)B_1''(r)+5\lambda r^2B_2(r)B_1''(r)+24\pi r^2\right.\\&B_2(r)B_1''(r)-3\gamma r^2B_1'(r)B_2'(r)-5\lambda r^2B_1'(r)B_2'(r)-24\pi r^2\\&B_1'(r)B_2'(r)+3\gamma rB_2(r)B_1'(r)+4\lambda rB_2(r)B_1'(r)+24\pi r\\&\times B_2(r)B_1'(r)-3\gamma rB_1(r)B_2'(r)-2\lambda rB_1(r)B_2'(r)\\&\left.-24\pi rB_1(r)B_2'(r)+2\lambda B_1(r)B_2(r)^3-2\lambda B_1(r)B_2(r)\right].\end{aligned} \tag{14}$$

At the center of a compact star, where $p_r(0)=p_t(0)$, anisotropy Π vanishes, creating the anisotropic force $\frac{2\Pi(r)}{r}$ that, depending on the relationship between p_t and p_r, may be either repulsive or attractive. By reducing density and pressure at the center, a certain force may cause the celestial body to expand, which might have an effect on nuclear fusion and the stellar life cycle as a whole. Under extreme conditions, inward gravitational pull can compress matter, significantly increasing its density and internal pressure, potentially leading to neutron star's or black hole's formation.

3 New relativistic models admitting Darmois matching criteria

Finding solutions to the field equations using multiple approaches have attracted a lot of attention from researchers working in this field of astrophysics. Now is the moment to address the problem of identifying viable solutions which can help in modeling relativistic objects. Although this problem has been approached in a variety of ways in the literature, we will concentrate on two well-behaved variations of the anisotropy that have worked well in discussing cosmic systems in GR. The following analysis shall use these constraints to find the solutions along with their detailed physical analysis.

3.1 Model 1

The system becomes under-determined as evident from Eqs. (12)–(14), containing five unknowns that require additional constraints for a unique solution. One method is to treat any two unknowns as free, however, the literature does not value this approach. The alternative strategy takes into account two restrictions at once. Consequently, the initial constraint corresponds to an established form of the radial metric component provided as [61,62]

$$B_2^2(r)=\frac{a+2br^2}{a+br^2}. \tag{16}$$

To maintain consistency, the dimension of the constants a and b must be null and $\frac{1}{\ell^2}$. These constants will be determined subsequently using matching criteria. When $B_2^2(r)$ is supplanted in Eq. (15) and reorganizing the terms, we get

$$\frac{B_1''(r)}{B_1(r)} - \frac{\left(a^2+4abr^2+2b^2r^4\right)B_1'(r)}{rB_1(r)\left(a^2+3abr^2+2b^2r^4\right)} = \frac{\Pi(\gamma+\lambda+8\pi)\left(a+2br^2\right)^2-2b^2r^2}{a^2+3abr^2+2b^2r^4}. \tag{17}$$

If a particular form of Π is provided, it is simple to solve Eq. (17) for $B_1(r)$. The anisotropic pressure profile must be carefully modeled to ensure a smooth, radially increasing distribution from the core to the boundary. A physically realistic solution typically requires an outward-increasing anisotropy to maintain stability. Expanding on this conversation, we take into account the following element that fits the previously described requirements

$$\Pi(r) = \frac{2b^2r^2}{(\gamma+\lambda+8\pi)\left(a+2br^2\right)^2}. \tag{18}$$

Swapping the above value into Eq. (17), we get

$$\frac{B_1''(r)}{B_1(r)} - \frac{\left(a^2+4abr^2+2b^2r^4\right)B_1'(r)}{rB_1(r)\left(a^2+3abr^2+2b^2r^4\right)} = 0. \tag{19}$$

The solution for $B_1(r)$, which is obtained by solving the overhead differential equation, is given by

$$B_1(r) = C_2 + \frac{C_1}{8b}\Big[4\sqrt{a+br^2}\sqrt{a+2br^2} - \sqrt{2}a\ln \times \left(2\sqrt{2}\sqrt{a+br^2}\sqrt{a+2br^2}+3a+4br^2\right)\Big], \tag{20}$$

where the integration constants C_1 and C_2 can be determined using boundary conditions. The following form expresses the field equations (12)–(14) under metric components (16) and (20) as

$$\begin{aligned}
\rho = {} & \Big[b\Big\{8bC_2(3\gamma+4\lambda+24\pi)\left(3a+2br^2\right)\left(12\sqrt{2}a^3+a^2\right. \\
& \times \left(52\sqrt{2}br^2+17\eta_1\right)+24abr^2\left(3\sqrt{2}br^2+2\eta_1\right) \\
& \left.+32b^2r^4\left(\sqrt{2}br^2+\eta_1\right)\right)+C_1\left(4\eta_1^2\left(17a^2+12a\right.\right. \\
& \times \left(4br^2+\sqrt{2}\eta_1\right)+16br^2\left(2br^2+\sqrt{2}\eta_1\right)\Big) \\
& \times \left(9a(\gamma+2\lambda+8\pi)+2br^2(3\gamma+10\lambda+24\pi)\right) \\
& -a(3\gamma+4\lambda+24\pi)\left(3a+2br^2\right) \\
& \times \left(24a^3+a^2\left(104br^2+17\sqrt{2}\eta_1\right)+48abr^2\right. \\
& \times \left(3br^2+\sqrt{2}\eta_1\right)+32b^2r^4\left(2br^2+\sqrt{2}\eta_1\right)\Big)\ln \\
& \left.\times \left(3a+4br^2+2\sqrt{2}\eta_1\right)\right)\Big\}\Big] \\
& \times \left[3\eta_1(\gamma+\lambda+8\pi)(\gamma+2\lambda+8\pi)\left(a+2br^2\right)^2\right. \\
& \times \left(3a+4br^2+2\sqrt{2}\eta_1\right)^2\Big\{C_1\left(4\eta_1-\sqrt{2}a\ln\right. \\
& \left.\times \left(3a+4br^2+2\sqrt{2}\eta_1\right)\right)+8bC_2\Big\}\Big]^{-1},
\end{aligned} \tag{21}$$

$$\begin{aligned}
p_r = {} & \Big[b\Big\{C_1\left(4\eta_1^2\left(17a^2+12a\left(4br^2+\sqrt{2}\eta_1\right)\right.\right. \\
& +16br^2\left(2br^2+\sqrt{2}\eta_1\right)\Big) \\
& \times \left(9a(\gamma+2\lambda+8\pi)+2br^2(9\gamma+14\lambda+72\pi)\right) \\
& +a\left(24a^3+a^2\left(104br^2+17\sqrt{2}\eta_1\right)\right. \\
& +48abr^2\left(3br^2+\sqrt{2}\eta_1\right) \\
& \left.+32b^2r^4\left(2br^2+\sqrt{2}\eta_1\right)\right)\left(3(\gamma+8\pi)\left(a+2br^2\right)\right. \\
& \left.+8b\lambda r^2\right)\ln\left(3a+4br^2+2\sqrt{2}\eta_1\right)\Big)-8bC_2\left(12\sqrt{2}a^3\right. \\
& +a^2\left(52\sqrt{2}br^2+17\eta_1\right)+24abr^2\left(3\sqrt{2}br^2+2\eta_1\right) \\
& +32b^2r^4\left(\sqrt{2}br^2+\eta_1\right)\Big)\left(3(\gamma+8\pi)\right. \\
& \times \left.\left(a+2br^2\right)+8b\lambda r^2\right)\Big\}\Big] \\
& \times \left[3(\gamma+\lambda+8\pi)(\gamma+2\lambda+8\pi)\left(a+2br^2\right)^2\right. \\
& \times \left(3a+4br^2+2\sqrt{2}\eta_1\right)^2\Big\{C_1\left(4\eta_1-\sqrt{2}a\ln\right. \\
& \left.\times \left(3a+4br^2+2\sqrt{2}\eta_1\right)\right)+8bC_2\Big\}\Big]^{-1},
\end{aligned} \tag{22}$$

$$\begin{aligned}
p_t = {} & \Big[b\Big\{8bC_2\left(12\sqrt{2}a^3+a^2\left(52\sqrt{2}br^2+17\eta_1\right)\right. \\
& +24abr^2\left(3\sqrt{2}br^2+2\eta_1\right)+32b^2r^4\left(\sqrt{2}br^2+\eta_1\right)\Big) \\
& \times \left(4b\lambda r^2-3a(\gamma+8\pi)\right)+C_1\left(4\eta_1^2\right. \\
& \times \left(17a^2+12a\left(4br^2+\sqrt{2}\eta_1\right)\right. \\
& \left.+16br^2\left(2br^2+\sqrt{2}\eta_1\right)\Big)\left(9a(\gamma+2\lambda+8\pi)\right. \\
& +8br^2(3\gamma+5\lambda \\
& \left.+24\pi)\right)+a\left(24a^3+a^2\left(104br^2+17\sqrt{2}\eta_1\right)\right. \\
& +48abr^2\left(3br^2+\sqrt{2}\eta_1\right) \\
& \left.+32b^2r^4\left(2br^2+\sqrt{2}\eta_1\right)\right)\left(3a(\gamma+8\pi)\right. \\
& \left.-4b\lambda r^2\right)\ln\left(3a+4br^2+2\sqrt{2}\eta_1\right)\Big)\Big\}\Big] \\
& \times \left[3(\gamma+\lambda+8\pi)(\gamma+2\lambda+8\pi)\left(a+2br^2\right)^2\right. \\
& \times \left(3a+4br^2+2\sqrt{2}\eta_1\right)^2 \\
& \times \left\{C_1\left(4\eta_1-\sqrt{2}a\ln\right.\right. \\
& \left.\times \left(3a+4br^2+2\sqrt{2}\eta_1\right)\right)+8bC_2\Big\}\Big]^{-1},
\end{aligned} \tag{23}$$

where $\eta_1 = \sqrt{a+br^2}\sqrt{a+2br^2}$.

Junction conditions play a vital role in analyzing compact stellar objects, as they govern how physical fields and their spatial derivatives transition across boundaries separating distinct regions or spacetime geometries. These prerequisites, which include the extrinsic curvature and metric continuity, guarantee the field equations' correctness and the smooth matching of spacetime areas. These prerequisites are necessary to solve boundary value issues, examine wave and disturbance propagation, and comprehend how physical structure behave at junctions. With respect to the inner spacetime (5), the Schwarzschild line element is obtained to

represent the external spacetime as

$$ds^2 = -\left(1-\tfrac{2M}{r}\right)dt^2 + \left(1-\tfrac{2M}{r}\right)^{-1}dr^2 + r^2(d\theta^2+\sin^2\theta d\phi^2), \tag{24}$$

with $r > 2M$ and M being the star's mass. The junction requirements consist of two fundamental aspects: intrinsic geometry's continuity, guaranteeing smooth metric tensor matching across the interface, and extrinsic curvature compatibility, governing the embedding relationship between adjacent spacetime regions. Furthermore, according to the later notion, the radial pressure must cease to exist at the star's radius $r = R$. These conditions result in three equations expressed by

$$1-\frac{2M}{R} = \frac{a+2bR^2}{a+bR^2}, \tag{25}$$

$$\sqrt{1-\frac{2M}{R}} = \frac{C_1}{8b}\big[4\sqrt{a+bR^2}\sqrt{a+2bR^2} - \sqrt{2}a\ln \times \big(2\sqrt{2}\sqrt{a+bR^2}\sqrt{a+2bR^2}+3a+4br^2\big)\big] + C_2, \tag{26}$$

$$\begin{aligned} p_r(R) = 0 = C_1\big\{&4\eta_2^2\big(17a^2+12a\big(4bR^2+\sqrt{2}\eta_2\big) \\ &+16bR^2\big(2bR^2+\sqrt{2}\eta_2\big)\big)\big(9a(\gamma+2\lambda+8\pi)+2bR^2 \\ &\times(9\gamma+14\lambda+72\pi)\big)+a\big(24a^3+a^2\big(17\sqrt{2}\eta_2 \\ &+104bR^2\big)+48abR^2\big(3bR^2+\sqrt{2}\eta_2\big)+32b^2R^4 \\ &\times\big(\sqrt{2}\eta_2+2bR^2\big)\big)\big(3(\gamma+8\pi)\big(a+2bR^2\big)+8b\lambda R^2\big) \\ &\times\ln\big(3a+4bR^2+2\sqrt{2}\eta_2\big)\big\}-8bC_2\big\{12\sqrt{2}a^3 \\ &+a^2\big(52\sqrt{2}bR^2+17\eta_2\big)+24abR^2\big(3\sqrt{2}bR^2+2\eta_2\big) \\ &+32b^2R^4\big(\sqrt{2}bR^2+\eta_2\big)\big\}\big\{3\big(a+2bR^2\big) \\ &\times(\gamma+8\pi)+8b\lambda R^2\big\}. \end{aligned} \tag{27}$$

The following expressions for the triplet (a, C_1, C_2) are obtained by solving Eqs. (25)–(27) simultaneously

$$a = \frac{-2bMR^2-bR^3}{2M}, \tag{28}$$

$$\begin{aligned} C_1 = \sqrt{1-\frac{2M}{R}}\big[&8b\big(12\sqrt{2}a^3+a^2\big(52\sqrt{2}bR^2+17\eta_2\big) \\ &+24abR^2\big(3\sqrt{2}bR^2+2\eta_2\big)+32b^2R^4\big(\sqrt{2}bR^2+\eta_2\big)\big) \\ &\times\big\{3(\gamma+8\pi)\big(a+2bR^2\big)+8b\lambda R^2\big\}\big] \\ &\times\big[24\eta_2^2(2\gamma+3\lambda+16\pi)\big(a+2bR^2\big) \\ &\times\big(17a^2+12a\big(4bR^2+\sqrt{2}\eta_2\big)+16bR^2 \\ &\times\big(2bR^2+\sqrt{2}\eta_2\big)\big)-a\big(24a^3+a^2\big(104bR^2+17\sqrt{2}\eta_2\big) \\ &+48abR^2\big(3bR^2+\sqrt{2}\eta_2\big)+32b^2R^4\big(2bR^2+\sqrt{2}\eta_2\big)\big) \\ &\times\big(3(\gamma+8\pi)\big(a+2bR^2\big)+8b\lambda R^2\big) \\ &\big\{\ln\big(3a+4br^2+2\sqrt{2}\eta_2\big) \\ &-\ln\big(3a+4bR^2+2\sqrt{2}\eta_2\big)\big\}\big]^{-1}, \end{aligned} \tag{29}$$

$$\begin{aligned} C_2 = \sqrt{1-\frac{2M}{R}}\big[&\big\{4\eta_2^2\big(17a^2+12a\big(4bR^2+\sqrt{2}\eta_2\big) \\ &+16bR^2\big(2bR^2+\sqrt{2}\eta_2\big)\big) \\ &\times\big(9a(\gamma+2\lambda+8\pi)+2bR^2(14\lambda \\ &+9\gamma+72\pi)\big)+a\big(24a^3+a^2\big(104bR^2+17\sqrt{2}\eta_2\big) \\ &+48abR^2\big(3bR^2+\sqrt{2}\eta_2\big)+32b^2R^4\big(2bR^2+\sqrt{2}\eta_2\big)\big) \\ &\times\big(3(\gamma+8\pi)\big(a+2bR^2\big)+8b\lambda R^2\big) \\ &\times\ln\big(3a+4bR^2+2\sqrt{2}\eta_2\big)\big\}\big] \\ &\times\big[24\eta_2(2\gamma+3\lambda+16\pi)\big(a+2bR^2\big)\big(17a^2+12a \\ &\times\big(4bR^2+\sqrt{2}\eta_2\big)+16bR^2\big(2bR^2+\sqrt{2}\eta_2\big)\big) \\ &-a\big(24a^3+a^2\big(104bR^2+17\sqrt{2}\eta_2\big) \\ &+48abR^2\big(3bR^2+\sqrt{2}\eta_2\big)+32b^2R^4 \\ &\times\big(2bR^2+\sqrt{2}\eta_2\big)\big)\big(3(\gamma+8\pi)\big(a+2bR^2\big)+8b\lambda R^2\big) \\ &\times\big\{\ln\big(3a+4br^2+2\sqrt{2}\eta_2\big) \\ &-\ln\big(3a+4bR^2+2\sqrt{2}\eta_2\big)\big\}\big]^{-1}, \end{aligned} \tag{30}$$

where $\eta_2 = \eta_1(R) = \sqrt{a+bR^2}\sqrt{a+2bR^2}$. These values will be used in the graphical analysis of our developed model. Incorporating the parameters γ and λ into the aforementioned constants would greatly facilitate our examination of how the alteration of gravitational theory affects the structural properties of celestial solutions.

3.2 Model 2

To determine if the resultant solution can accurately represent physically actual compact structures, we consider a particular version of the g_{rr} metric potential. This metric component has been used in GR earlier, presenting valid results. Here, we examine its coherence within the context of modified theory. This is given as follows [63]

$$B_2^2(r) = \frac{f\left(h+2r^2\right)}{\left(f-r^2\right)\left(h+r^2\right)}, \tag{31}$$

with the dimensions of both constants f and h being $\frac{1}{\ell^2}$. Equation (15) is simplified to when $B_2^2(r)$ is substituted as

$$\Pi(r)=\frac{B_1'(r)\{hr^4-f(h^2+4hr^2+2r^4)\}+r(f-r^2)(h^2+3hr^2+2r^4)B_1''(r)+r^3B_1(r)(2f+h)}{frB_1(r)(\gamma+\lambda+8\pi)(h+2r^2)^2}. \tag{32}$$

On rearranging Eq. (32), we obtain

$$\frac{B_1'(r)\{hr^4-f(h^2+4hr^2+2r^4)\}}{rB_1(r)(f-r^2)(h^2+3hr^2+2r^4)}+\frac{B_1''(r)}{B_1(r)}=\frac{f\Pi(\gamma+\lambda+8\pi)(h+2r^2)^2-r^2(2f+h)}{(f-r^2)(h^2+3hr^2+2r^4)}. \tag{33}$$

Given a specified anisotropy's profile, the temporal metric potential can be determined. In this context, we examine several options for Π and try to resolve Eq. (33) and deduce one viable option which is presented as

$$\Pi(r)=\frac{r^2(2f+h)}{f(\gamma+\lambda+8\pi)(h+2r^2)^2}. \tag{34}$$

It is evident that the factor (34) is an appropriate choice as it has a zero value at the star's center and rises approaching toward the exterior. Upon putting this into Eq. (33), we get

$$\frac{B_1'(r)\{hr^4-f(h^2+4hr^2+2r^4)\}}{rB_1(r)(f-r^2)(h^2+3hr^2+2r^4)}+\frac{B_1''(r)}{B_1(r)}=0, \tag{35}$$

which is a differential equation of second order in $B_1(r)$ whose analytical solution is taken out as

$$\begin{aligned}B_1(r)=&\frac{C_3\sqrt{r^2-f}}{\sqrt{h+r^2}\sqrt{h+2r^2}}\sqrt{\frac{h+2r^2}{r^2-f}}\\&\times\left\{(h+r^2)\sqrt{\frac{h+2r^2}{r^2-f}}+\sqrt{-2f-h}\right.\\&\times\sqrt{r^2-f}\sqrt{\frac{h+r^2}{r^2-f}}\\&\left.\times E\left(\sin^{-1}\left(\frac{\sqrt{-f-\frac{h}{2}}}{\sqrt{r^2-f}}\right)\middle|\frac{2(f+h)}{2f+h}\right)\right\}+C_4,\end{aligned} \tag{36}$$

with the integration constants C_3 and C_4. Additionally, we put both (31) and (36) into Eqs. (12)–(14) to obtain the fluid triplet's final form and present them in Appendix A.

In order to use the matching criterion, the spacetime must be asymptotically smooth and static outside of a spherical star. While examining model 1, we used the Schwarzschild metric (24). At $r=R$, the two basic forms lead to the following equations

$$1-\frac{2M}{R}=\frac{(f-R^2)(h+R^2)}{f(h+2R^2)}, \tag{37}$$

$$\begin{aligned}\sqrt{1-\frac{2M}{R}}=&\frac{1}{\sqrt{h+R^2}\sqrt{h+2R^2}}\left[C_3\sqrt{R^2-f}\right.\\&\times\sqrt{\frac{h+2R^2}{R^2-f}}\left\{(h+R^2)\sqrt{\frac{h+2R^2}{R^2-f}}\right.\\&+\sqrt{R^2-f}E\left(\sin^{-1}\left(\frac{\sqrt{-f-\frac{h}{2}}}{\sqrt{R^2-f}}\right)\middle|\right.\\&\left.\left.\left.\times\frac{2(f+h)}{2f+h}\right)\sqrt{-2f-h}\sqrt{\frac{h+R^2}{R^2-f}}\right\}\right]+C_4,\end{aligned} \tag{38}$$

$$\begin{aligned}p_r(R)=0=&\sqrt{-2f-h}\sqrt{R^2-f}\big(3(\gamma+8\pi)\\&\times(h+2R^2)(f+h+R^2)+4\lambda R^2(2f+h)\big)\\&\times E\left(\sin^{-1}\left(\frac{\sqrt{-f-\frac{h}{2}}}{\sqrt{R^2-f}}\right)\middle|\frac{2(f+h)}{2f+h}\right)\\&+\left((h+R^2)\sqrt{\frac{h+2R^2}{R^2-f}}\big(\lambda\big(18R^4-9fh\right.\\&-10fR^2+13hR^2\big)-3(\gamma+8\pi)\\&\left.\times(h+2R^2)(f-h-3R^2)\big)\right)\left(\frac{h+R^2}{R^2-f}\right)^{-1/2}\\&-C_4(R^2-f)^{3/2}\sqrt{h+R^2}\sqrt{h+2R^2}\sqrt{\frac{h+R^2}{R^2-f}}\\&\times\sqrt{\frac{h+2R^2}{R^2-f}}\big(3(\gamma+8\pi)(h+2R^2)\\&\times(f+h+R^2)+4\lambda R^2(2f+h)\big).\end{aligned} \tag{39}$$

Equations (37)–(39) yield the three constants as

$$f=\frac{R^3(h+R^2)}{2hM+R^2(4M-R)}, \tag{40}$$

$$C_3 = -\frac{\sqrt{1-\frac{2M}{R}}\left\{3(\gamma+8\pi)\left(h+2R^2\right)\left(f+h+R^2\right)+4\lambda R^2(2f+h)\right\}}{3(2\gamma+3\lambda+16\pi)\sqrt{R^2-f}\sqrt{h+R^2}\left(h+2R^2\right)^{3/2}}, \tag{41}$$

$$\begin{aligned} C_4 = \sqrt{1-\frac{2M}{R}}\Bigg[\Bigg\{&\sqrt{\frac{h+2R^2}{R^2-f}} \\ &\times \big(3(\gamma+8\pi)\big(h+2R^2\big)\big(f+h+R^2\big) \\ &+4\lambda R^2(2f+h)\Big)\Bigg(\big(h+R^2\big)\sqrt{\frac{h+2R^2}{R^2-f}} \\ &+\sqrt{-2f-h}\sqrt{R^2-f}\sqrt{\frac{h+R^2}{R^2-f}}E \\ &\times\left(\sin^{-1}\left(\frac{\sqrt{-f-\frac{h}{2}}}{\sqrt{R^2-f}}\right)\middle|\frac{2(f+h)}{2f+h}\right)\Bigg)\Bigg\} \\ &\times\left\{3(2\gamma+3\lambda+16\pi)\big(h+R^2\big)\right. \\ &\left.\times\big(h+2R^2\big)^2\right\}^{-1}+1\Bigg]. \end{aligned} \tag{42}$$

Notably, the triplet (f, C_3, C_4) is expressed in terms of h, suggesting it to be a free parameter. In the subsequent section, these values shall be used to assess the developed model's (A1)–(A3) stability.

4 Graphical exploration of essential physical features

This section presents a comprehensive visual analysis of the obtained solutions, examining their internal properties and assessing their structural viability. The objective is assessing the result's responses under various stresses and physical circumstances in order to provide light on their stability. To assess the physical viability of our solutions, we first analyze core properties including: the behavior of matter variables, and the regularity of metric components. The specific tests and methods shall be used to assess these attributes in the next subsections. It is essential to note that our analysis employs specific parameter values within the considered theoretical framework, namely $\gamma = \{0.1, 1.6\}$ and $\lambda = \{0, 0.2, 0.4, 0.6, 0.8, 1\}$, with the stellar candidate 4U 1820-30, which has radius $R = 9.1 \pm 0.2km$ and mass $M = 1.58 \pm 0.09 M_{\odot}$ [64]. This data has been used to examine how the modified model under investigation affects the existence of stellar solutions.

Notably, the selection of 4U 1820-30 is motivated by its well-established observational constraints, which make it an ideal candidate for testing theoretical models of compact stars. This pulsar, observed in the globular cluster NGC 6624, is a well-studied neutron star with precise measurements derived from X-ray observations. Its mass and radius fall within the typical range for neutron stars, providing a realistic benchmark for assessing the viability of our anisotropic solutions in $f(R, L_m, T)$ gravity. Furthermore, the considered data is consistent with the constraints imposed by recent astrophysical observations, such as those from the Neutron Star Interior Composition Explorer (NICER) and gravitational wave events like GW170817, which favor neutron stars with masses around $1.4 - 2.0 M_{\odot}$ and radii in the range of $9 - 14km$. By choosing 4U 1820-30, we ensure that our theoretical models are tested against a physically relevant and observationally well-constrained object, enhancing the applicability of our results to real astrophysical systems. We also confirm that our models are designed to accurately reproduce the observational values of 4U 1820-30 within error margins, through the application of the Darmois matching conditions. These conditions ensure continuity of the metric and its derivatives across the stellar boundary, as well as the vanishing of radial pressure at the surface. By solving the resulting system of equations for both models, we determine the constants such that the mass and radius of the star align with the observed values of 4U 1820-30. Specifically, the Schwarzschild exterior metric is matched to the interior solutions at $r = R$, ensuring that the total mass is recovered at the boundary. The error margins ($\pm 0.09 M_{\odot}$ for mass and $\pm 0.2km$ for radius) are accounted for in our numerical computations.

4.1 Metric functions and consistency of fluid sector

At the center of the star, both the g_{tt} and g_{rr} metric coefficient must remain constant and unity, respectively, thereafter increasing outward. Furthermore, they must be finite and positive across the whole interior domain. In model 1, these elements are defined at the center as

$$\begin{aligned} B_1^2(0) &= \left[C_2 - \frac{aC_1\left\{\sqrt{2}\ln\left(\left(3+2\sqrt{2}\right)a\right)-4\right\}}{8b}\right]^2 \\ &= constant, \quad B_2^2(0) = 1, \end{aligned}$$

and, in contrast, the components of model 2 are structured as follows

$$B_1^2(0) = \Big[C_3\Big\{\sqrt{-2f-h}E$$

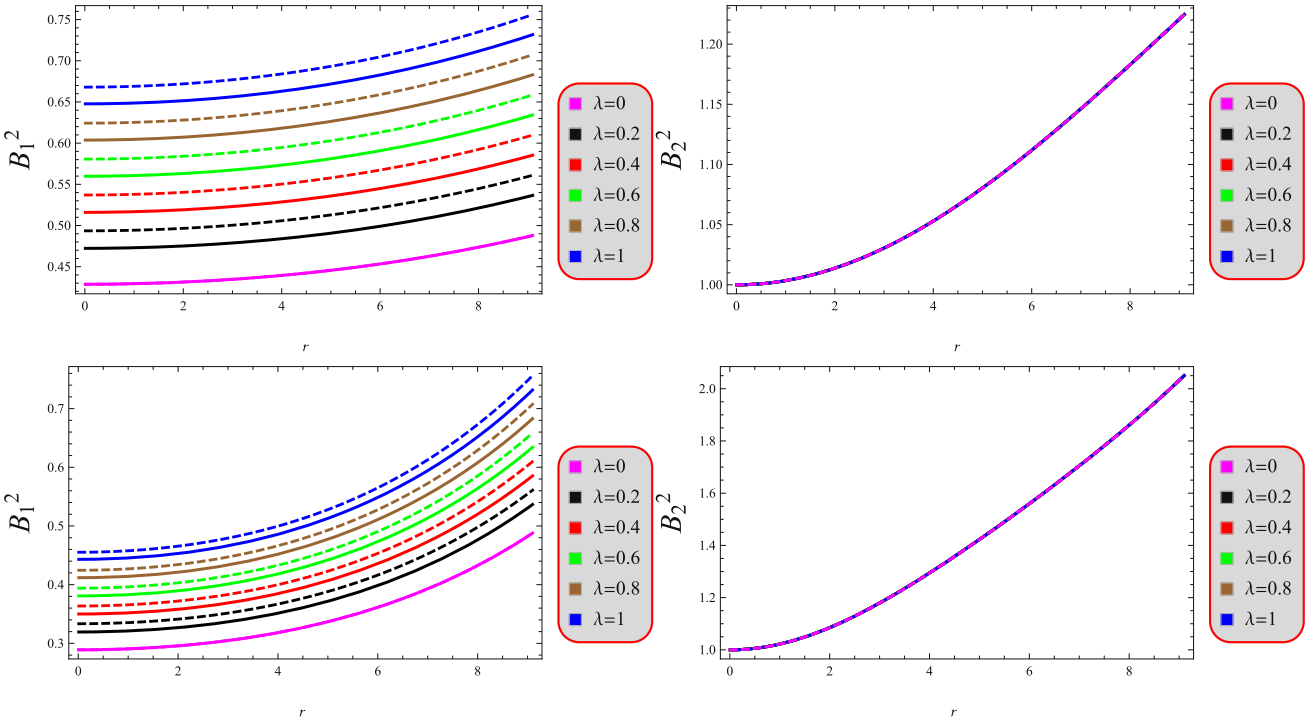

Fig. 1 Geometric quantities for both novel solutions (upper plots for model 1 and lower for 2). Also, $\gamma = 0.1$ corresponds to solid and 1.6 to dashed lines

$$\times \left(\sin^{-1}\left(\frac{\sqrt{-f-\frac{h}{2}}}{\sqrt{-f}} \right) \left| \frac{2(f+h)}{2f+h} \right. \right) + \frac{h}{\sqrt{-f}} \Bigg\} + C_4 \Bigg]^2$$
$$= constant, \quad B_2^2(0) = 1.$$

All these elements satisfy the regularity condition at the coordinate origin, ensuring physical consistency. As shown in Fig. 1, they maintain strictly positive and well-defined profiles.

The fluid parameters' characteristics are essential to comprehending the system's stability and structure. From the core to the boundary, the density has to be positive, finite, and decreasing. The radial and tangential pressures must have positive and highest values in the core and subsequently decrease outward. Anisotropy may arise when transverse pressure differs from the radial pressure. According to the description above, Fig. 2 displays each of these elements. The density shows an inverse relationship with parameters γ and λ, revealing systematically lower densities compared to standard GR predictions. Upon comparison of both models, it is evident that the model 2 yields less dense astral objects, while the $f(R,T)$ theory produces a denser configuration than the considered framework. This tendency is equally applicable to transverse and radial pressures. The latter pressure ingredient is determined to be null at $r = R$. The last row of Fig. 2 shows the anisotropy to be zero at $r = 0$ because the pressures are the same there. The rising behavior of this quantity signifies the creation of enough external pressure that sustains the model's stability under the gravitational force.

To provide a quantitative comparison, we analyze the impact of the $f(R, L_m, T)$ model on the density and pressure profiles of the compact star 4U 1820-30, relative to $f(R)$ and $f(R,T)$ models, focusing on percentage deviations in these quantities. For the $f(R)$ model, we consider a linear form $f(R) = R + \alpha R^2$, and for $f(R,T)$, we use $f(R,T) = R + \beta T$, as these are the closest analogs to our model for a fair comparison. In the $f(R)$ model, the field equations reduce to those of GR for $\alpha = 0$, leading to a rescaling of the density and pressure terms. For a typical value of $\alpha = 0.1$, the density in the $f(R)$ model is approximately 10% higher than in GR at the stellar core due to the enhanced curvature contributions, assuming a similar metric ansatz to our model 1. In contrast, the $f(R,T)$ model, with $\beta = 0.4$, introduces a T-dependent term that reduces the central density by approximately 5–8% compared to GR, as the trace T contributes negatively to the effective EMT, particularly in regions of high anisotropy. For our $f(R, L_m, T)$ model, with $\gamma = 0.1$ and $\lambda = 0.4$, the density at the core of 4U 1820-30 is approximately 15% lower than in the $f(R)$ model and 7% lower than in the $f(R,T)$ model. This reduction arises because the L_m term counteracts the curvature and T contributions, leading to a less dense core. Specifically, at $r = 0$, the $f(R, L_m, T)$ model yields a central density of approximately $3.5 \times 10^{14} g/cm^3$, com-

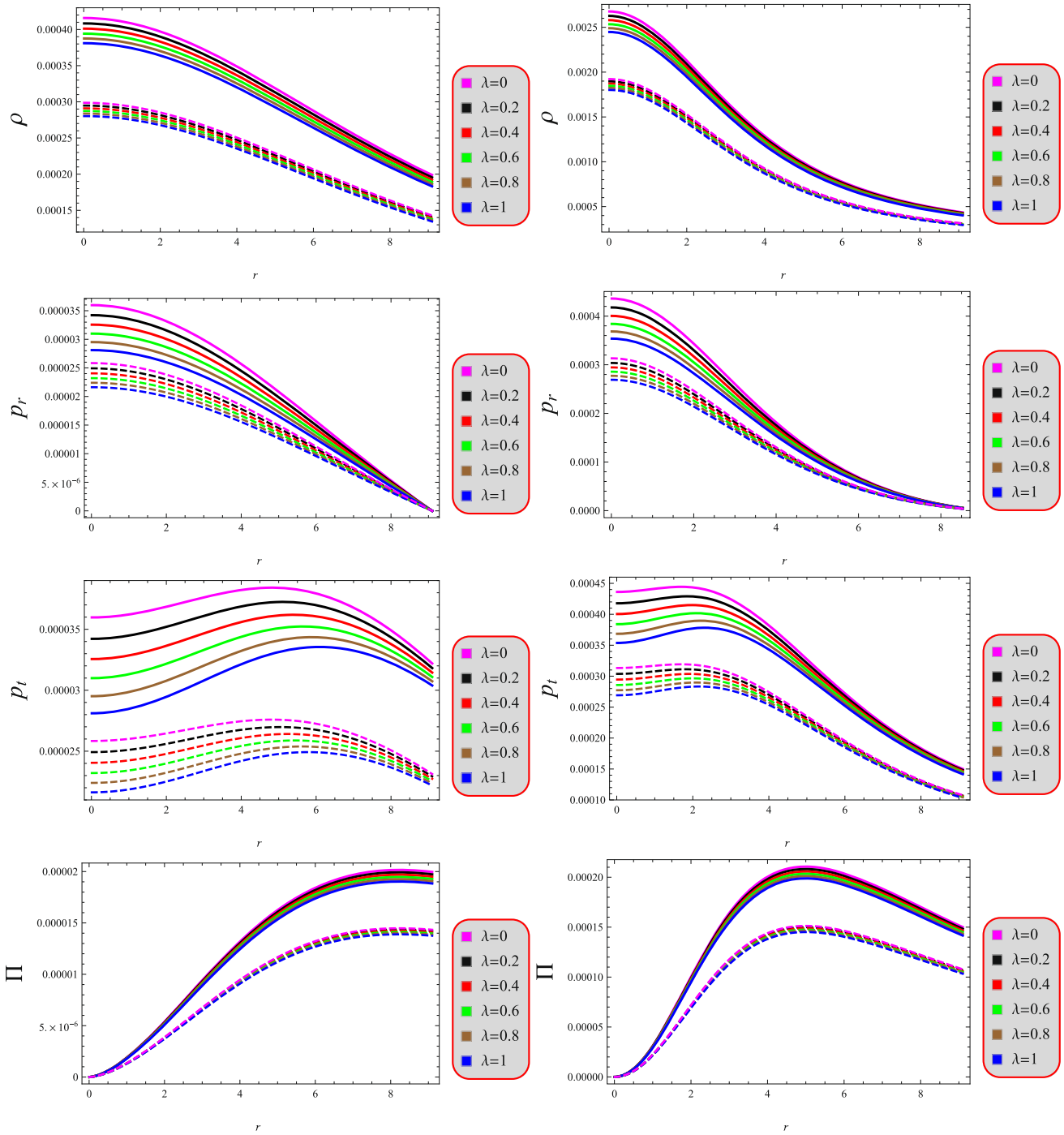

Fig. 2 Fluid variables for both novel solutions (left plots for model 1 and right for 2). Also, $\gamma = 0.1$ corresponds to solid and 1.6 to dashed lines

pared to $4.1 \times 10^{14} g/cm^3$ in $f(R)$ and $3.8 \times 10^{14} g/cm^3$ in $f(R, T)$ for the same metric parameters. For radial pressure, the $f(R, L_m, T)$ model shows a central value of approximately $2.5 \times 10^{34} dyn/cm^2$, which is 12% lower than the $f(R)$ model's $2.8 \times 10^{34} dyn/cm^2$ and 6% lower than the $f(R, T)$ model's $2.7 \times 10^{34} dyn/cm^2$. These differences are most pronounced near the core, where the matter-geometry coupling is strongest, and diminish toward the surface, where p_r approaches zero due to boundary conditions. The lower density and pressure in the model (8) have significant implications for the stability and structure of anisotropic stars. The reduced central density suggests that this model can support stable configurations with less extreme matter distributions, potentially aligning better with observational constraints on neutron star equations of state. The presence of both γ and λ terms allows for fine-tuning of the anisotropic

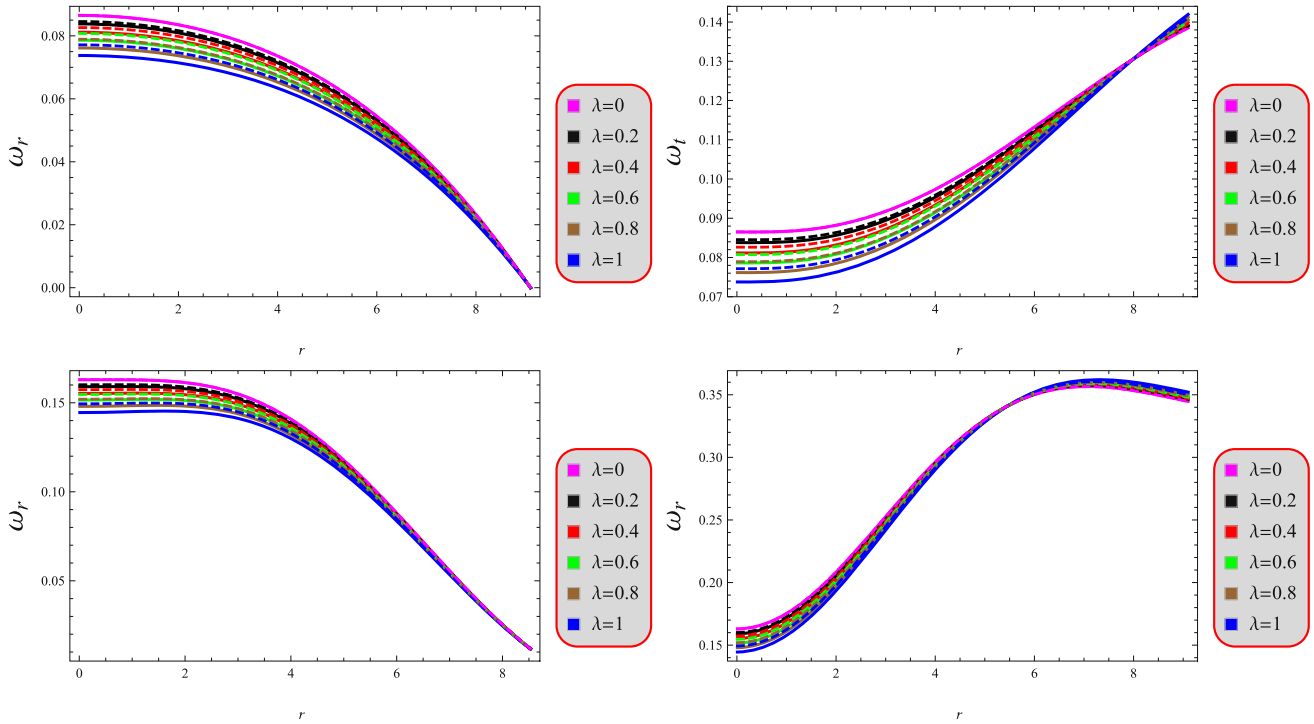

Fig. 3 Two parameters associated with equation of state for both novel solutions (upper plots for model 1 and lower for 2). Also, $\gamma = 0.1$ corresponds to solid and 1.6 to dashed lines

pressure profile. This flexibility is absent in $f(R)$ models, where anisotropy is purely a function of the metric and fluid properties, and partially limited in $f(R,T)$ models, where only T contributes to deviations from GR.

4.2 Equation of state

The equation of state is given by $p_i = \omega_i \rho$, where ω_i with $i = t, r$ represents the transverse and radial components. They are articulated as follows

$$\omega_r = \frac{p_r}{\rho}, \quad \omega_t = \frac{p_t}{\rho}. \tag{43}$$

The ratios of pressure ingredients to energy density must fall between [0, 1] for a fluid structure to be physically valid. Meeting this condition guarantees thermodynamic consistency within the stellar core, adhering to essential physical laws governing compact objects. Figure 3 unequivocally illustrates that both parametric values are less than unity, indicating that energy density prevails over pressures inside the self-gravitational entity. This suggests that as one approaches the star's surface, the fluid characteristics show a steadily declining trend.

4.3 Some mass-related physical factors

The mass that is contained inside a sphere of radius r is determined by

$$\begin{aligned} m(r) &= 4\pi \int_0^r r^2 \rho(r) dr \\ \implies & m'(r) = 4\pi r^2 \rho(r). \end{aligned} \tag{44}$$

The aforementioned differential equation may be solved either numerically or analytically, contingent upon intricacy of the density's formulation. Figure 4 shows the mass function profile, demonstrating that as r approaches zero, $m(r)$ also vanishes. On the other hand, this function has a consistently growing behavior outside.

An object's stability and gravitational binding are significantly influenced by its compactness, which is determined by the ratio of mass and radius. Highly dense entities, like neutron stars, demonstrate significant gravitational influences. Buchdahl [65] asserted that the non-dimensional compactness factor $\left(\mu(r) = \frac{m(r)}{r}\right)$ must not exceed 0.44 to maintain a feasible compact structure. Although initially derived for spherically symmetric isotropic systems, subsequent research has verified this condition's validity for anisotropic matter distributions. The surface redshift phenomenon, characterized by gravitational wavelength elongation of emitted radiation, directly correlates with stellar compactness. This occurs as photons lose energy and overcome

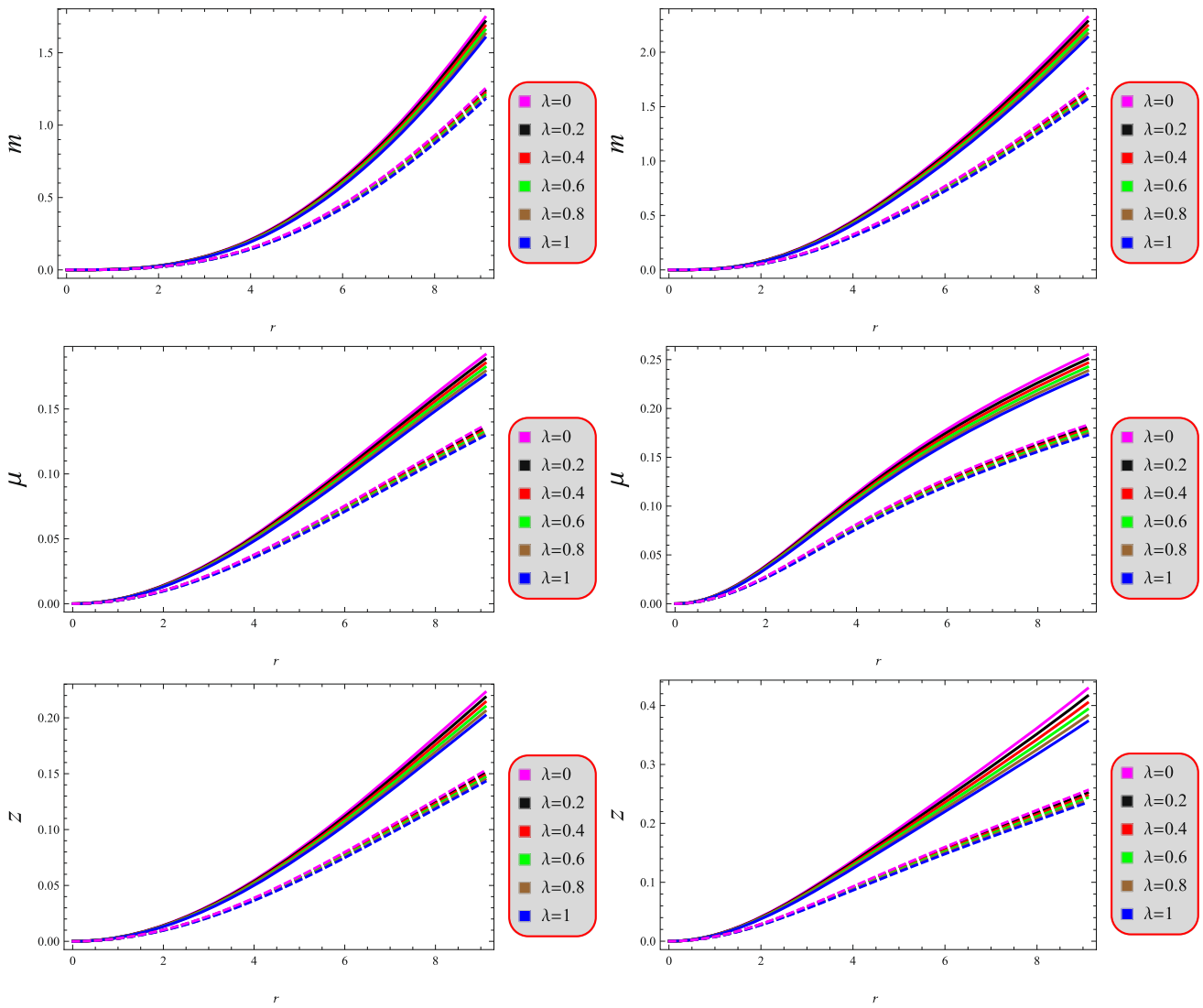

Fig. 4 Physical factors for both novel solutions (left plots for model 1 and right for 2). Also, $\gamma = 0.1$ corresponds to solid and 1.6 to dashed lines

the star's gravitational potential. This is given by

$$z = \left\{1 - 2\mu(r)\right\}^{-\frac{1}{2}} - 1, \tag{45}$$

showing that the compactness and redshift are closely interconnected. For anisotropic configurations, the surface redshift reaches a theoretical maximum of 5.211 at the stellar boundary [66], a critical constraint for physical viability. These parameters are presented in Fig. 4, demonstrating an adequate profile over the entire domain.

4.4 Viability conditions

To construct a feasible star model, certain requirements, namely energy conditions (ECs) should be fulfilled. These may be divided into four categories which are expressed below. Imposing these circumstances enables investigators to examine the characteristics of the fluid inside the star interior, determining either it is standard or unconventional. By imposing these limitations, investigators may ascertain boundaries of density and pressure, ensuring the hypothetical model corresponds with empirical observations. They are represented as follows

Dominant ECs: $\rho \pm p_r \geq 0, \quad \rho \pm p_t \geq 0,$

Null ECs: $\rho + p_r \geq 0, \quad \rho + p_t \geq 0,$

Strong ECs: $\rho + p_r \geq 0, \quad \rho + p_t \geq 0, \quad \rho + p_r + 2p_t \geq 0,$

Weak ECs: $\rho \geq 0, \quad \rho + p_r \geq 0, \quad \rho + p_t \geq 0.$

Given that all matter parameters shown in Fig. 2 are positive, it suffices to analyze the conditions $\rho - p_t \geq 0$ and $\rho - p_r \geq 0$ to ascertain the model's feasibility. These bounds are shown in Fig. 5 whose consistently favorable profile suggests the presence of a conventional fluid in stellar interiors, thus allowing us to assert that our solutions are viable.

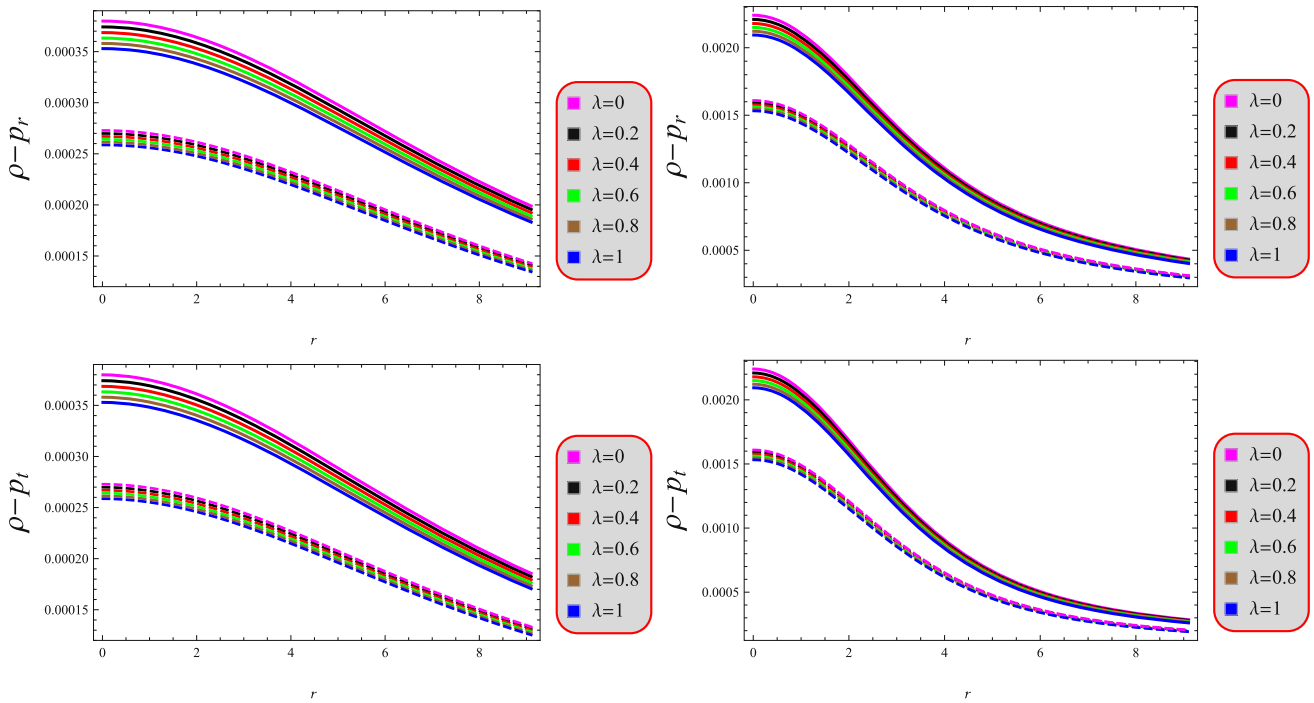

Fig. 5 Viability for both novel solutions (left plots for model 1 and right for 2). Also, $\gamma = 0.1$ corresponds to solid and 1.6 to dashed lines

5 Stability exploration

Stability analysis represents a fundamental validation step in compact star modeling, determining whether derived solutions correspond to physically realizable astrophysical configurations. The methodology focuses on analyzing equilibrium configurations of degenerate stellar remnants – particularly neutron stars and white dwarfs – while assessing their stability against radial perturbations. Utilizing various mathematical methods, scientists may ascertain the circumstances that enable these stars to sustain stability or experience significant transformations. Certain evaluation tests are implemented in the following subsections.

5.1 Tolman–Oppenheimer–Volkoff equations

Here, we analyze the equilibrium state of both developed models under diverse forces influencing our system [63,67]. The equilibrium equation in this modified theory may include four forces which are discussed below. In this theory, there exist a non-zero divergence of the conventional EMT. Consequently, an additional force manifests inside the gravitational field of a self-gravitating body, altering the geodesic trajectories of test particles. The Tolman-Oppenheimer-Volkoff equations may be expressed mathematically as

$$\nabla^{\alpha} T_{\alpha\beta} = \frac{1}{8\pi + 2f_T + f_{L_m}} \times \Bigg[\nabla_{\beta}\{(2f_T + f_{L_m})L_m\} - T_{\alpha\beta}\nabla^{\alpha}(2f_T + f_{L_m}) - (f_T \nabla_{\beta} T + f_{L_m} \nabla_{\beta} L_m) - 8\pi \nabla^{\alpha} \xi_{\alpha\beta} - 4g^{\zeta\mu}\nabla^{\alpha}\left(f_T \frac{\partial^2 L_m}{\partial g^{\alpha\beta}\partial g^{\zeta\mu}}\right)\Bigg], \tag{46}$$

which becomes under the considered model (8) as

$$p_r' + \frac{B_1'(r)\,(p_r + \rho)}{B_1(r)} + \frac{\lambda\left(p_r' + 2p_t' + \rho'\right)}{2\lambda + 2\gamma + 8\pi} - \frac{2\,(p_t - p_r)}{r} = 0. \tag{47}$$

The four kinds of forces derived from the aforementioned equation are designated as: gravitational f_g, anisotropic f_a, hydrostatic f_h, and the force associated with modified gravity f_m. To maintain the balance of all theses forces to get the net some to be zero, the following condition must be fulfilled

$$f_{\text{total}} = f_g + f_a + f_h + f_m = 0, \tag{48}$$

where

$$f_a = \frac{2\,(p_t - p_r)}{r}, \quad f_g = -\frac{B_1'(r)}{B_1(r)}\,(p_r + \rho)\,,$$
$$f_h = -p_r', \quad f_m = -\frac{\lambda\left(p_r' + 2p_t' + \rho'\right)}{2\lambda + 2\gamma + 8\pi}.$$

Figure 6 shows that both our models are in equilibrium state as the net sum of all four forces becomes zero.

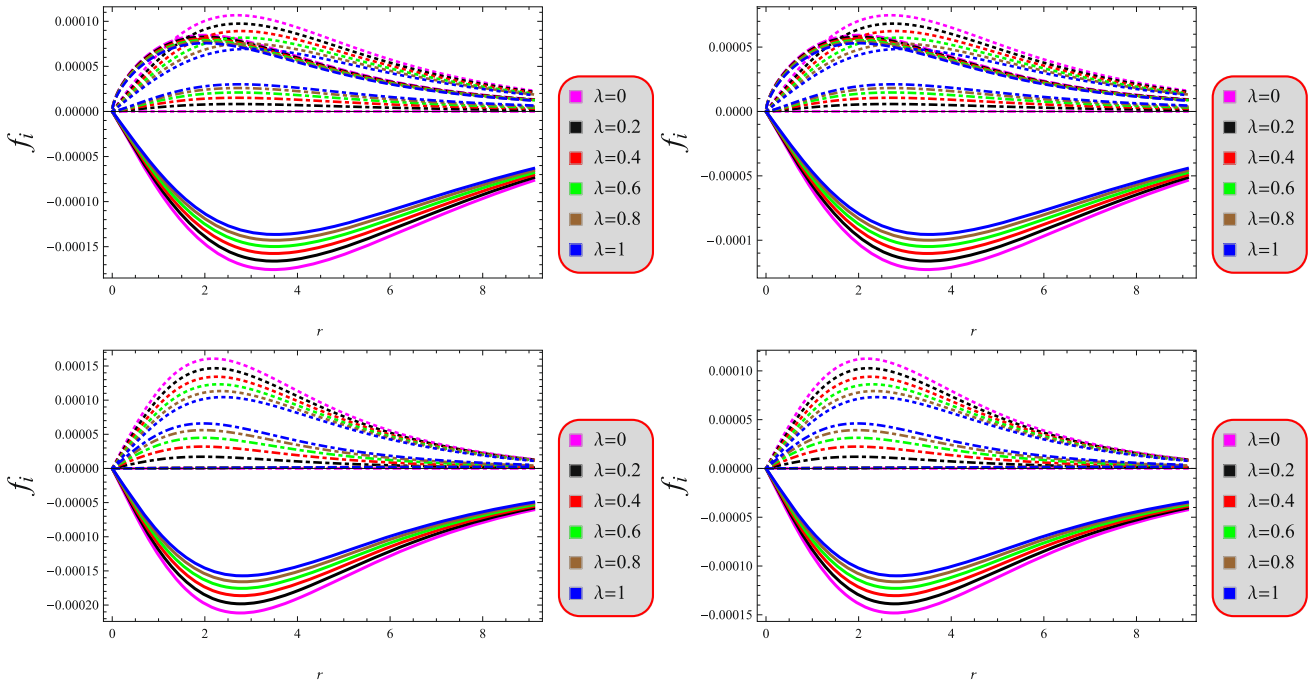

Fig. 6 Equilibrium of forces (f_g (solid), f_h (doted), f_a (dashed) and f_m (dot-dashed)) for both novel solutions (left plots for model 1 and right for 2). Also, upper plots correspond to $\gamma = 0.1$ and lower plots to 1.6

5.2 Causality, cracking and adiabatic index

According to the causality criterion, information cannot spread more quickly than light. In the examination of massive anisotropic stars, this condition establishes limitations to tangential and radial sound velocities, ensuring that the sound speed inside the star remains inferior to the light speed at any point inside the internal spacetime [68]. As per the mathematically perspective, we define

$$0 \leq v_t^2 = \frac{dp_t}{d\rho} \leq 1, \quad 0 \leq v_r^2 = \frac{dp_r}{d\rho} \leq 1.$$

This criteria is graphically shown in Figure 7 for both newly constructed models and we see this to be satisfied for all selections of the relevant parameters. Therefore, our solutions exhibit stability under this extended gravitational theory.

Another method for investigating potentially stable anisotropic topologies is to assess the existence or deficiency of cracking within the internal dispersion. The primary assertion is that the fluid constituents speed up in relation to each other on both sides of the fracture site. This process is essential for insight the manner of fluid dispersion after its departure from the condition of equilibrium. Herrera [69] was the first to examine the phenomenon of cracking in the context of self-gravitational collapsar. The cracking condition stipulates that the component $|v_t^2 - v_r^2|$ must reside inside the unit interval to guarantee stability. The final two plots in Fig. 7 illustrate this factor, demonstrating that this requirement is valid for both models, hence, indicating their stable profile over all parametric values.

The adiabatic index serves as a critical parameter in modeling compact stellar objects, governing their stability against gravitational collapse. It illustrates relationship between density and pressure variations in a matter source under adiabatic circumstances, when heat transfer is absent. For a stable compact star, the adiabatic index must exceed $\frac{4}{3}$ [70,71]. When the stability parameter drops below this critical value, gravitational collapse becomes energetically favorable, leading to stellar instability. This component is ascertained as

$$\Gamma_t = \frac{\rho + p_t}{p_t}\frac{dp_t}{d\rho}, \quad \Gamma_r = \frac{\rho + p_r}{p_r}\frac{dp_r}{d\rho}.$$

Figure 7 graphically illustrates the aforementioned factors, demonstrating that both models provide stable solutions by fulfilling the criterion that the factors Γ_r and Γ_t exceed $\frac{4}{3}$.

6 Brief discussion of our results

We conduct a detailed graphical analysis in Sects. 4 and 5, particularly, using the observational data of the compact star 4U 1820-30. Figures 1, 2, 3, 4, 5, 6 and 7 illustrate the behavior of the fluid parameters, the equation of state parameters, mass, compactness, redshift, energy conditions, sound velocities, and adiabatic indices for certain parametric choices.

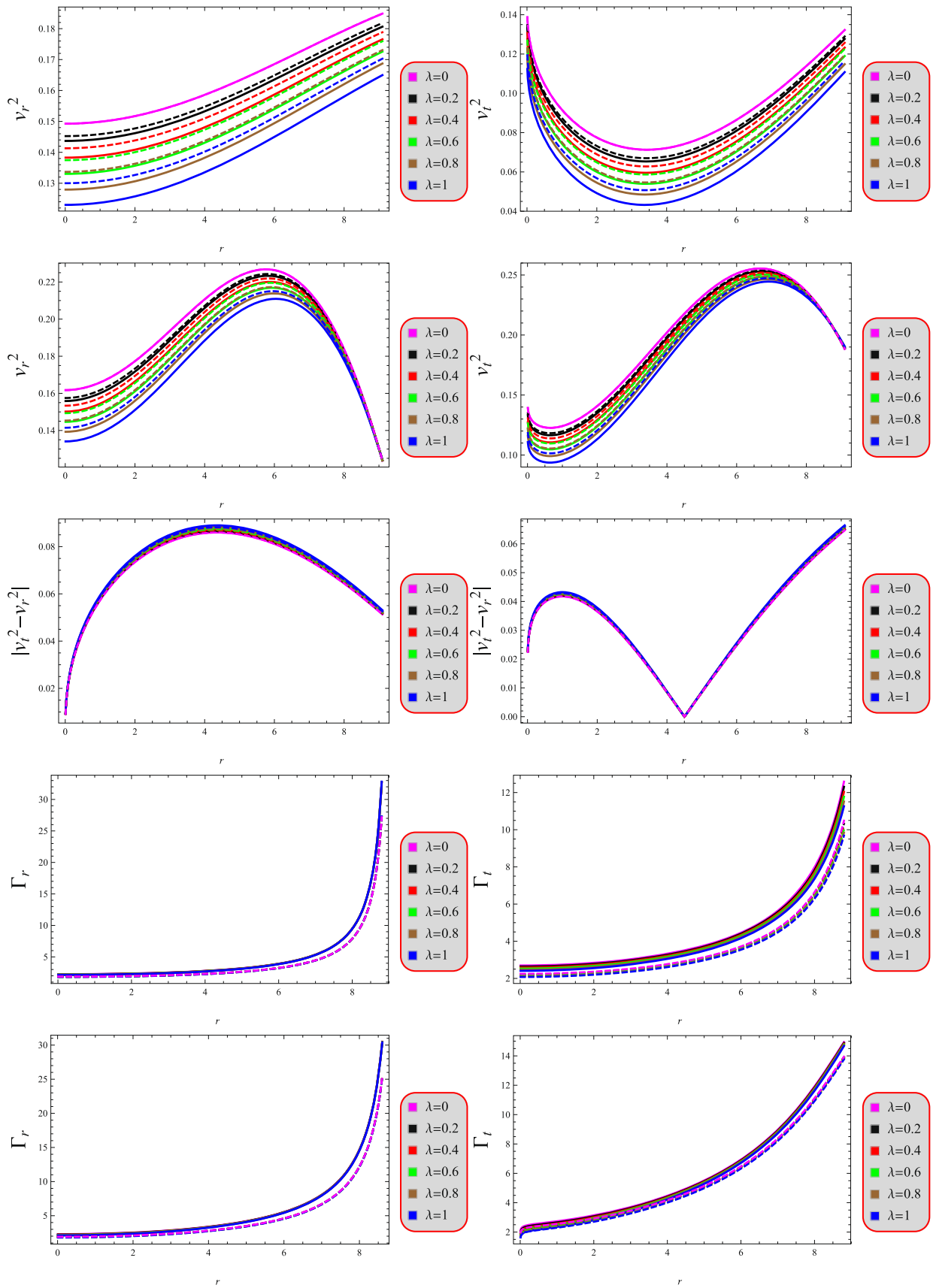

Fig. 7 Stability for both novel solutions (left plots for model 1 and right for 2). Also, $\gamma = 0.1$ corresponds to solid and 1.6 to dashed lines

To further clarify, we observe that increasing γ and λ systematically reduces the density and pressure profiles compared to GR. For instance, in Fig. 2, the density for both models decreases as these parameters increase, with model 2 exhibiting lower densities than model 1. This trend suggests that the matter-geometry coupling in $f(R, L_m, T)$ gravity dilutes the matter concentration relative to GR, likely due to the additional effective terms in the EMT that modify the gravitational interaction. The radial and tangential pressures exhibit similar behavior, with higher values of parameters leading to lower pressure profiles. Notably, the radial pressure satisfies the physical requirement of vanishing at the stellar boundary, which is ensured by the boundary conditions. The anisotropy also responds to changes in γ and λ, with larger values of these parameters resulting in a slightly reduced anisotropic factor. This indicates that the coupling parameters modulate the directional dependence of pressure, influencing the repulsive forces that counteract gravitational collapse. The equation of state parameters remain within the physically acceptable range [0, 1] for all parametric values, confirming thermodynamic consistency. However, increasing γ and λ tends to lower these ratios, suggesting a softer equation of state, which impacts the compressibility of the stellar matter. The mass function, compactness, and redshift further illustrate the influence of these parameters. The mass profile increases monotonically with radius, but higher parametric values result in a slightly lower total mass at the boundary, reflecting the reduced density. The compactness factor remains below the Buchdahl limit of 0.44, and the surface redshift adheres to the theoretical maximum of 5.211, ensuring physical viability across all parameter choices. The energy conditions (Fig. 5), equilibrium of forces (Fig. 6), sound velocities, and adiabatic indices (Fig. 7) all confirm the stability and feasibility of both models, with γ and λ variations causing subtle shifts in the profiles but not violating any physical constraints.

To provide a more explicit quantification, we note that for $\gamma = 0.1$ and $\lambda = 0$, the density at the center of the star in model 1 is approximately 0.0004 km^{-2}, while for $\gamma = 1.6$ and $\lambda = 1$, it drops to around 0.00015 km^{-2}. Similarly, in model 2, the central density decreases from approximately 0.0025 km^{-2} to 0.0005km^{-2} as γ and λ increase. These reductions, on the order of 60–80%, highlight the significant role of the matter-geometry coupling in altering the stellar structure. The pressures follow a comparable trend, with central values decreasing by similar percentages, which directly affects the equation of state and stability parameters. These quantitative changes are consistent across both models, with model 2 generally producing less dense configurations, likely due to the different functional form of the radial metric potential.

7 Conclusions

This research derives two novel exact solutions within the $f(R, L_m, T)$ gravity formalism, demonstrating new mathematical representations of coupled curvature-matter dynamics. The associated field equations have been established in this regard in relation to a static sphere which helped us in computing the corresponding anisotropy. The system contains five unknowns (two metric potentials and three matter variables) governed by four coupled differential equations (three Einstein field equations along with the anisotropy), requiring one additional physical constraint to achieve a unique solution. We have thus employed two well-defined, singularity-free ansatz for the g_{rr} component which generated coupled second-order differential equations governing the g_{tt} potential. We further examined different choices for the pressure anisotropy to aid in solving these equations, guaranteeing that the anisotropy component is null at the core and escalates outside. This mathematical formulation resulted in two separate compact star models. Afterwards, we used the Schwarzschild metric to ascertain the constants related to the metric potentials by using the boundary conditions. The condition $p_r(R) = 0$ was also imposed to determine the integration constants, thereby fixing all model parameters through this physical requirement. A comprehensive graphic examination of generated models has been performed under $\gamma = \{0.1, 1.6\}$ and $\lambda = \{0, 0.2, 0.4, 0.6, 0.8, 1\}$. The main results of this investigation are detailed below.

- The metric potentials g_{rr} and their corresponding g_{tt} components are clearly defined, exhibiting the anticipated behavior near the origin $r = 0$ and showing a gradual increase as they extend radially outward (Fig. 1). The fluid parameters satisfy the necessary conditions for the formation of dense celestial bodies, as illustrated in Fig. 2. The anisotropy vanishes at the center and grows radially outward, indicating a repulsive force that counteracts gravitational force, preventing collapse and ensures stellar stability.
- The equation of state effectively explains the matter dispersion's properties, with our analysis confirming the values of both associated parameters to lie within the physically meaningful range of 0 to 1 (Fig. 3). Both the compactness factor and redshift exhibit monotonic growth with radial distance, attaining peak values at the stellar boundary. The mass profile demonstrates a radially increasing behavior, attaining its maximum at the surface while converging to zero at the stellar center (Fig. 4).
- The physical viability of our solutions is confirmed through full compliance with all ECs (Fig. 5). Our mod-

els are also shown to be in equilibrium as all four forces balance each other for all parametric values (Fig. 6).

- The variations in transverse and radial sound velocity, together with the presence of cracking, indicate that our models exhibit feasibility irrespective of the selected parametric values. Likewise, the stability of these models is corroborated by the adiabatic criterion (Fig. 7).

Our models satisfy several crucial physical features and feasibility requirements inside the interiors of the pulsar 4U 1820-30, which is an important indicator for the presence of astronomical bodies in any gravitating theory. Our findings correspond with those of GR for both charged [47] and uncharged [59,60] situations. Consequently, the modify $f(R, L_m, T)$ gravitational endorses the possibility of dense models contingent upon certain choices of model parameters. Ultimately, when we assign γ and λ the zero value, our results converge with those of GR.

Acknowledgements The authors extend their appreciation to the Deanship of Scientific Research at Northern Border University, Arar, KSA for funding this work through the project number NBU-FFR-2025-3021-10. This work was supported by Princess Nourah bint Abdulrahman University Researchers Supporting Project number (PNURSP2025R59), Princess Nourah bint Abdulrahman University, Riyadh, Saudi Arabia.

Data Availability Statement No new data is generated in this study.

Code Availability Statement This manuscript has no associated code/software. [Authors' comment: Code/Software sharing not applicable to this article as no code/software was generated or analysed during the current study.]

Funded by SCOAP[3].

Appendix A

When we put Eqs. (31) and (36) into the system (12)–(14), the fluid triplet becomes

$$\rho = \Bigg[\sqrt{r^2-f}\sqrt{\frac{h+2r^2}{r^2-f}}\Bigg\{C_4(3\gamma+4\lambda+24\pi)$$
$$\times (r^2-f)^{3/2}\sqrt{h+r^2}\sqrt{h+2r^2}\sqrt{\frac{h+r^2}{r^2-f}}$$
$$\times \sqrt{\frac{h+2r^2}{r^2-f}}\big(r^2(2f+7h)$$
$$+3h(f+h)+6r^4\big)+C_3\big(h+r^2\big)\big(h+2r^2\big)$$
$$\times\Bigg(\big((h+r^2)\sqrt{\frac{h+2r^2}{r^2-f}}\big(3(\gamma+8\pi)$$
$$\times\big(r^2(2f+7h)+3h(f+h)+6r^4\big)+\lambda\big(r^2(14f$$
$$+25h)+3h(5f+4h)+18r^4\big)\big)\Big(\frac{h+r^2}{r^2-f}\Big)^{-1/2}$$
$$+(3\gamma+4\lambda+24\pi)\sqrt{-2f-h}\sqrt{r^2-f}\big(2f+7h\big)$$
$$\times r^2+3h(f+h)+6r^4\big)$$
$$\times E\Bigg(\sin^{-1}\Bigg(\frac{\sqrt{-f-\frac{h}{2}}}{\sqrt{r^2-f}}\Bigg)\Bigg|\frac{2(f+h)}{2f+h}\Bigg)\Bigg)\Bigg\}\Bigg]$$
$$\times\Bigg[3f(\gamma+\lambda+8\pi)(\gamma+2\lambda+8\pi)\big(h+2r^2\big)^3$$
$$\times\sqrt{\frac{f+h}{r^2-f}+1}\Bigg\{C_4\big(r^2-f\big)\sqrt{h+r^2}\sqrt{h+2r^2}$$
$$+C_3\Bigg(\sqrt{r^2-f}\big(h+r^2\big)\big(h+2r^2\big)+\sqrt{-2f-h}$$
$$\times\big(f-r^2\big)^2\sqrt{\frac{f+h}{r^2-f}+1}\sqrt{\frac{2f+h}{r^2-f}+2}$$
$$\times E\Bigg(\sin^{-1}\Bigg(\frac{\sqrt{-f-\frac{h}{2}}}{\sqrt{r^2-f}}\Bigg)\Bigg|\frac{2(f+h)}{2f+h}\Bigg)\Bigg)\Bigg\}\Bigg]^{-1}, \quad \text{(A1)}$$

$$p_r = \Bigg[\sqrt{r^2-f}\sqrt{\frac{h+2r^2}{r^2-f}}\Bigg\{C_3\big(-h-r^2\big)\big(h+2r^2\big)$$
$$\times\Bigg(\sqrt{-2f-h}\sqrt{r^2-f}\big(3(\gamma+8\pi)$$
$$\times\big(h+2r^2\big)\big(f+h+r^2\big)+4\lambda r^2(2f+h)\big)$$
$$\times E\Bigg(\sin^{-1}\Bigg(\frac{\sqrt{-f-\frac{h}{2}}}{\sqrt{r^2-f}}\Bigg)\Bigg|\frac{2(f+h)}{2f+h}\Bigg)$$
$$+\big((h+r^2)\sqrt{\frac{h+2r^2}{r^2-f}}\big(\lambda\big(-9fh-10fr^2+13hr^2$$
$$+18r^4\big)-3(\gamma+8\pi)\big(h+2r^2\big)\big(f-h-3r^2\big)\big)\big)$$
$$\times\Bigg(\frac{h+r^2}{r^2-f}\Bigg)^{-1/2}\Bigg)-C_4\big(r^2-f\big)^{3/2}\sqrt{h+r^2}\sqrt{h+2r^2}$$
$$\times\sqrt{\frac{h+r^2}{r^2-f}}\sqrt{\frac{h+2r^2}{r^2-f}}\big(3(\gamma+8\pi)\big(h+2r^2\big)$$
$$\times\big(f+h+r^2\big)+4\lambda r^2(2f+h)\big)\Bigg\}\Bigg]$$

$$\times\left[3f(\gamma+\lambda+8\pi)(\gamma+2\lambda+8\pi)\big(h+2r^2\big)^3\right.$$
$$\times\sqrt{\frac{f+h}{r^2-f}+1}\Big\{C_4\big(r^2-f\big)\sqrt{h+r^2}\sqrt{h+2r^2}$$
$$+C_3\Big(\sqrt{r^2-f}\big(h+r^2\big)\big(h+2r^2\big)+\big(f-r^2\big)^2$$
$$\times\sqrt{-2f-h}\sqrt{\frac{f+h}{r^2-f}+1}\sqrt{\frac{2f+h}{r^2-f}+2}E\Big(\sin^{-1}$$
$$\left.\times\left(\frac{\sqrt{-f-\frac{h}{2}}}{\sqrt{r^2-f}}\right)\Big|\frac{2(f+h)}{2f+h}\right)\Big)\Big\}\Big]^{-1}, \tag{A2}$$

$$p_t=\Big[\sqrt{r^2-f}\sqrt{\frac{h+2r^2}{r^2-f}}\Big\{C_3\big(-h-r^2\big)\big(h+2r^2\big)$$
$$\times\Big(\big((h+r^2\big)\sqrt{\frac{h+2r^2}{r^2-f}}$$
$$\times\big(\lambda\big(18r^4-9fh-22fr^2+7hr^2\big)$$
$$-3(\gamma+8\pi)\big(4r^2(f-h)+h(f-h)-6r^4\big)\big)\Big)$$
$$\times\left(\frac{h+r^2}{r^2-f}\right)^{-1/2}+\sqrt{-2f-h}\sqrt{r^2-f}\big(3(\gamma+8\pi)$$
$$\big(h(f+h)+2hr^2+2r^4\big)-2\lambda r^2(2f+h)\big)$$
$$\times E\Big(\sin^{-1}\left(\frac{\sqrt{-f-\frac{h}{2}}}{\sqrt{r^2-f}}\right)\Big|\frac{2(f+h)}{2f+h}\Big)\Big)$$
$$-C_4\big(r^2-f\big)^{3/2}\sqrt{h+r^2}\sqrt{h+2r^2}$$
$$\times\sqrt{\frac{h+r^2}{r^2-f}}\sqrt{\frac{h+2r^2}{r^2-f}}\big(3(\gamma+8\pi)\big(h(f+h)$$
$$\left.+2hr^2+2r^4\big)-2\lambda r^2(2f+h)\big)\Big\}\right]$$
$$\times\Big[3f(\gamma+\lambda+8\pi)\big(h+2r^2\big)^3(\gamma+2\lambda+8\pi)$$
$$\times\sqrt{\frac{f+h}{r^2-f}+1}\Big\{C_4\big(r^2-f\big)\sqrt{h+r^2}\sqrt{h+2r^2}+C_3$$
$$\times\Big(\sqrt{r^2-f}\big(h+r^2\big)\big(h+2r^2\big)+\big(f-r^2\big)^2$$
$$\times\sqrt{-2f-h}\sqrt{\frac{f+h}{r^2-f}+1}\sqrt{\frac{2f+h}{r^2-f}+2}$$
$$\times E\Big(\sin^{-1}\left(\frac{\sqrt{-f-\frac{h}{2}}}{\sqrt{r^2-f}}\right)\Big|\frac{2(f+h)}{2f+h}\Big)\Big)\Big\}\Big]^{-1}. \tag{A3}$$

References

1. K. Schwarzschild, Sitz. Deut. Akad. Wiss Berlin Kl. Math. Phys. **24**, 424 (1916)
2. K. Schwarzschild, Sitz. Deut. Akad. Wiss Berlin Kl. Math. Phys. **1916**, 189 (1916)
3. S. Capozziello, A. Stabile, A. Troisi, Class. Quantum Gravity **25**, 085004 (2008)
4. S. Nojiri, S.D. Odintsov, D. Sáez-Gómez, Phys. Lett. B **681**, 74 (2009)
5. A.V. Astashenok, S. Capozziello, S.D. Odintsov, J. Cosmol. Astropart. Phys. **01**, 001 (2015)
6. U. Debnath, N.U. Molla, A. Pradhan, Int. J. Geom. Methods Mod. Phys. **20**, 2350214 (2023)
7. A. Dixit, V.K. Bhardwaj, A. Pradhan, S. Krishnannair, Indian J. Phys. **97**, 3695 (2023)
8. O. Bertolami, C.G. Boehmer, T. Harko, F.S.N. Lobo, Phys. Rev. D **75**, 104016 (2007)
9. T. Harko, F.S.N. Lobo, Eur. Phys. J. C **70**, 373 (2010)
10. A. Pradhan, D.C. Maurya, G.K. Goswami, A. Beesham, Int. J. Geom. Methods Mod. Phys. **20**, 2350105 (2023)
11. M. Zeyauddin, A. Dixit, A. Pradhan, Int. J. Geom. Methods Mod. Phys. **21**, 2450038 (2024)
12. A. Dixit, A. Pradhan, M. Zeyauddin, J. Singh, Int. J. Mod. Phys. A **39**, 2450043 (2024)
13. T. Harko et al., Phys. Rev. D **84**, 024020 (2011)
14. C.P. Singh, P. Kumar, Eur. Phys. J. C **74**, 11 (2014)
15. E.H. Baffou et al., Astrophys. Space Sci. **356**, 173 (2015)
16. P. Kumar, C.P. Singh, Astrophys. Space Sci. **357**, 120 (2015)
17. P.H.R.S. Moraes, J.D.V. Arbañil, M. Malheiro, J. Cosmol. Astropart. Phys. **06**, 005 (2016)
18. A. Pradhan, A. Dixit, G. Varshney, Int. J. Mod. Phys. A **37**, 2250121 (2022)
19. G.G.L. Nashed, Astrophys. J. **950**, 129 (2023)
20. A. Pradhan, G. Goswami, A. Beesham, Int. J. Geom. Methods Mod. Phys. **20**, 2350169 (2023)
21. Y. Feng et al., Phys. Scr. **99**, 085034 (2024)
22. Z. Haghani, T. Harko, Eur. Phys. J. C **81**, 615 (2021)
23. T. Naseer, J.L. Said, Eur. Phys. J. C **84**, 808 (2024)
24. M. Zubair et al., Fortschr. Phys. **71**, 2300018 (2023)
25. S. Arora, P.H.R.S. Moraes, P.K. Sahoo, Eur. Phys. J. Plus **139**, 542 (2024)
26. P.H.R.S. Moraes, A.S. Agrawal, B. Mishra, Phys. Lett. B **855**, 138818 (2024)
27. J.Z. Pretel, Phys. Scr. **99**, 085001 (2024)
28. Y. Feng et al., Chin. J. Phys. **90**, 372–386 (2024)
29. T. Tangphati, I. Sakalli, A. Banerjee, A. Pradhan, Chin. Phys. C **49**, 025110 (2025)
30. C.E. Mota, J.M.Z. Pretel, C.O.V. Flores, Eur. Phys. J. C **84**, 673 (2024)
31. A. Rehman et al., Nucl. Phys. B **1013**, 116852 (2025)
32. A. Rehman et al., Nucl. Phys. B **1015**, 116897 (2025)
33. L. Herrera, N.O. Santos, Phys. Rep. **286**, 53 (1997)
34. J. Ovalle, Phys. Rev. D **95**, 104019 (2017)
35. M.R. Shahzad, G. Abbas, Int. J. Geom. Methods Mod. Phys. **16**, 1950132 (2019)
36. J. Ospino, L.A. Núñez, Eur. Phys. J. C **80**, 166 (2020)
37. L. Herrera, A. Di Prisco, J. Ospino, E. Fuenmayor, J. Math. Phys. **42**, 2129 (2001)
38. J.H. Jeans, Mon. Not. R. Astron. Soc. **82**, 122 (1922)
39. M. Ruderman, Annu. Rev. Astron. Astrophys. **10**, 427 (1972)
40. V. Canuto, Annu. Rev. Astron. Astrophys. **12**, 167 (1974)
41. R. Ciolfi, V. Ferrari, L. Gualtieri, Mon. Not. R. Astron. Soc. **406**, 2540 (2010)
42. R.F. Sawyer, Phys. Rev. Lett. **29**, 382 (1972)
43. V. Canuto, Annu. Rev. Astron. Astrophys. **12**, 167 (1974)
44. H. Heiselberg, M. Hjorth-Jensen, Phys. Rep. **328**, 237 (2000)
45. R.L. Bowers, E.P.T. Liang, Astrophys. J. **188**, 657 (1974)
46. H.C. Das, Phys. Rev. D **106**, 103518 (2022)
47. M. Sharif, T. Naseer, Eur. Phys. J. Plus **139**, 296 (2024)

48. A. Caliskan et al., J. High Energy Astrophys. **44**, 99–115 (2024)
49. K. Hassan et al., Chin. J. Phys. **91**, 916–931 (2024)
50. B. Siza et al., Eur. Phys. J. C **84**, 1203 (2024)
51. G. Murtaza et al., J. High Energy Astrophys. **44**, 279–289 (2024)
52. B. Rasheed et al., Int. J. Geom. Methods Mod. Phys. **22**, 2450302 (2025)
53. G. Mustafa et al., Nucl. Phys. B **1012**, 116812 (2025)
54. A. Ashraf et al., Nucl. Phys. B **1014**, 116873 (2025)
55. G. Mustafa et al., Eur. Phys. J. C **85**, 575 (2025)
56. J. Andrade et al., Eur. Phys. J. C **85**, 598 (2025)
57. A. Ashraf et al., Eur. Phys. J. C **85**, 633 (2025)
58. S.S.C. Medina et al., Eur. Phys. J. C **85**, 722 (2025)
59. L. Baskey, S. Ray, S. Das, S. Majumder, A. Das, Eur. Phys. J. C **83**, 307 (2023)
60. S. Das, K. Chakraborty, F. Rahaman, S. Majumder, Eur. Phys. J. C **84**, 527 (2024)
61. M. Kohler, K.L. Chao, Z. Naturforsch. A **20**, 1537 (1965)
62. R.S. Tikekar, Curr. Sci. **39**, 460 (1970)
63. R.C. Tolman, Phys. Rev. **55**, 364 (1939)
64. T. Güver, P. Wroblewski, L. Camarota, F. Ozel, Astrophys. J. **719**, 1807 (2010)
65. H.A. Buchdahl, Phys. Rev. **116**, 1027 (1959)
66. B.V. Ivanov, Phys. Rev. D **65**, 104011 (2002)
67. J.R. Oppenheimer, G.M. Volkoff, Phys. Rev. **55**, 374 (1939)
68. H. Abreu, H. Hernández, L.A. Núñez, Class. Quantum Gravity **24**, 4631 (2007)
69. L. Herrera, Phys. Lett. A **165**, 206 (1992)
70. S. Chandrasekhar, Astrophys. J. **140**, 417 (1964)
71. H. Heintzmann, W. Hillebrandt, Astron. Astrophys. **38**, 51 (1975)